Experiment 614 (including Experiment 1111) TWIST

(G. Marshall, TRIUMF; R. MacDonald, Alberta)

In 2006, the TRIUMF weak interaction symmetry test (TWIST, Expt. 614) obtained most of the data required for its final results. Essentially all of the available beam time was devoted to acquiring data sets with high statistical significance and well-controlled systematic influences. Variations in the beam and detector were minimized by improvements to monitoring, control, and analysis systems, based on the experience gained in prior running periods. The year also saw the publication of a new TWIST physics paper [Jamieson *et al.*, Phys. Rev. **D74**, 072007-1 (2006)] and an instrumentation paper [Hu *et al.*, Nucl. Instrum. Methods **A566**, 563 (2006)] describing the construction and use of a detector for muon beam monitoring. It was also decided to propose and carry out a separate experiment (Expt. 1111) using the muon spin relaxation apparatus and infrastructure of the TRIUMF Centre for Molecular and Materials Science.

TWIST is an experiment to measure the positive muon decay spectrum to extract precise values of three of the four decay ("Michel") parameters, ρ, δ, and $\mathcal{P}_\mu\xi$. If the results differ from predictions of the standard model (SM) of particle physics, the deviations indicate contributions from physics beyond the SM. For example, more precise limits for ρ and $\mathcal{P}_\mu\xi$ establish more restrictive limits on possible parameters of a left-right symmetric (LRS) model, i.e., mixing angle ζ and mass m_2 of a heavier gauge boson partner W_2 which mediates right-handed interactions. The goal of TWIST is to determine the three decay parameters simultaneously with experimental precision better than one part per thousand (10^{-3}), to achieve an approximately tenfold improvement over results of prior experiments. To do this, TWIST uses a high-precision, low-mass, planar detector array in a 2 T solenoidal magnetic field. It measures tracks of positrons from muon decay to record distributions of momentum and angle with respect to muon polarization direction.

Physics accomplishments

The first round of physics results, published in 2005, represented an improvement of more than a factor of two over previous measurements of ρ [Musser *et al.*, Phys. Rev. Lett. **94**, 101805 (2005)] and δ [Gaponenko *et al.*, Phys. Rev. **D71**, 071101(R) (2005)]. These results set new limits on the right-handed coupling of the muon in a model independent way, as well as squeezing the parameter space for certain classes of extensions to the SM. A more refined analysis of data taken in 2004 continued during 2006 to improve the precision of the previous results for ρ and δ. It features a reduction in several important systematic uncertainties as well as an increase in the fiducial region in decay angle and momentum over which the decay parameters are fit. The analysis incorporates a better helix fit algorithm which accounts for positron energy loss and allows kinks arising from multiple scattering. The space-time relationships of the TWIST drift chambers have been tested and made more precise, with more realistic and detailed cell geometry for both simulation and data analysis. Energy calibration has improved due to a better understanding of the processes involved, with the help of a more sophisticated decay endpoint energy determination algorithm. Positron interaction systematics have been studied in greater detail, and a more accurate muon beam characterization (based on the TEC; see below) has been implemented for the new analysis.

In 2006, another physics paper was published [Jamieson *et al., op. cit.*] on the quantity $\mathcal{P}_\mu\xi$, where ξ is the muon decay parameter describing the asymmetry of the decay spectrum, and $\mathcal{P}_\mu$ is the degree of muon polarization in pion decay. The new result agrees with previous measurements but is more than a factor of two more precise. The consequence of TWIST data on mass and mixing angle parameters in the LRS model is shown in Fig. 1.

The measurement required many careful studies of muon depolarization, to understand, minimize, and compensate for it. In that analysis, dominant limitations from two distinct sources of depolarization were encountered, due to beam passing through the fringe field and due to a small amount of muon spin relaxation after stopping in the high purity metal TWIST target. To overcome those limitations, data taking in 2006 included some aspects which will be described below.

Improvements to data-taking

Following experience in the operation of the muon beam monitoring detector, the time expansion chamber system (TPC) [Hu *et al., op. cit.*] was used to great advantage in 2006. Placed near the entrance to the solenoid where fringe fields can cause significant depolarization (Fig. 2), it monitors the beam position and angle in both transverse horizontal and vertical directions. Each incoming particle is measured, allowing us to build an accurate beam profile in a matter of minutes. The TEC had shown in 2005 that the incident muon beam was deflected from the ideal spectrometer axis by the solenoid fringe field and its interaction with nearby M13 beam elements. The deflection was substantial, causing significant depolarization of the muon beam and an unacceptably high sensitivity of the depolarization to small beam instabilities. Extra small power supplies were added to provide an asymmetric

field (a dipole component) in three quadrupoles (Q4, Q6, and Q7) in M13; in conjunction with the normal adjustable horizontal deflection of B2, the asymmetric current could be used to compensate for the deflection in both horizontal and vertical directions. By determining the beam response to the deflecting currents, it was possible to correct the mean positions and angles of the incoming muons in order to reduce depolarizing transverse momentum components near the fringe field and within the detector. After optimizing the path of the muon beam through the fringe field, the depolarization is near a minimum and becomes less sensitive to small changes in the beam position.

Because the TEC causes the beam polarization to be slightly reduced due to multiple scattering prior to the fringe field, it is typically removed for data-taking. In order to monitor the average muon transverse momentum continuously, the mean muon beam positions in the planes of the TWIST detector were monitored and fit to a helical trajectory. This provides a figure of merit for maintaining maximum polarization (with minimum instability) of the beam on its path to the stopping target. Projections of the trajectories are shown in Fig. 3 for a beam steered away from the solenoid magnetic axis, and in Fig. 4 following a procedure to reduce transverse momentum and hence depolarization. The difference shows the degree to which mean transverse momentum can be reduced.

While improvements to the beam as well as understanding and control of its behaviour in the fringe field are expected to reduce the dominant systematic uncertainty for $\mathcal{P}_\mu\xi$ (3.4×10^{-3} in the result reported in Jamieson *et al.* [*op. cit.*] by a factor of perhaps five, there remains the uncertainty due to depolarization of muons following thermalization in TWIST muon stopping targets. Target depolarization is spin relaxation due to magnetic interactions with the target material prior to the time of muon decay, which must be accounted for by an extrapolation to the muon arrival time. In Jamieson *et al.* [*op. cit.*] an uncertainty in this extrapolation resulted in a systematic uncertainty of 1.2×10^{-3}. In an attempt to improve the precision of the extrapolation and to verify the time dependence of relaxation in Al and Ag, a proposal was approved as Expt. 1111 for a dedicated experiment using the facilities of TRIUMF's Centre for Molecular and Materials Science (CMMS) with a muon spin rotation apparatus on the M20 beam. Two weeks of data were taken in December. Results are still being analyzed, but so far they justify the extrapolation of TWIST data at times >1 μs back to the arrival time. No clear distinction can yet be made about the functional form (exponential vs. Gaussian) of the relaxation.

Many other improvements have been made to the experiment. In order to confirm that the results for decay parameters do not depend on the target material, a high purity (99.999% Ag, thickness 0.027 mm) silver target was installed, replacing the high purity (99.999% Al, thickness 0.072 mm) aluminum one. More variables, some derived from a fast analysis of 1% of the data stream, were added to the long list of histograms which are regularly checked for stability. Graphite target operation still presents some problems, especially as the targets age and begin to produce a radioactive beam gas background for the spectrometer. This is also monitored so that the target failure can be more readily foreseen.

Progress in analysis

There are several improvements to the analysis that have been developed or implemented in 2006. The relative time calibration of the drift chambers is now done routinely as real data are being taken, whereas previously we relied on calibration runs with solenoid field off, before and after a long period of data-taking. A method to extract from data a relationship of time to distance from drift chamber wires is nearing completion. By applying it to both real data and simulation, the possibility of bias in the track fitting algorithms should be reduced. In addition, the extracted relations can be used to simulate and account for many temperature, pressure, and chamber geometry effects. Energy calibration, which is required to be accurate to a few parts in ten thousand, has presented many challenges, but significant progress was made as new and improved algorithms have been investigated. A test of alignment procedures is in progress, with the goal of verifying our procedures and reducing the related systematic uncertainties. There are several aspects to alignment; drift chamber plane relative transverse and relative rotational alignments, alignment of the angle of the detector axis to the solenoid magnetic axis, alignment of the transverse detector position to the solenoid and beam axes, TEC alignment, and so on. Each requires a procedure using a certain type of data.

The future of TWIST

TWIST is nearing the end of data-taking. Barring surprises, we expect to finish in 2007, but the analysis will extend at least into 2008. The analysis routines are not yet ready to begin the final pass at data, but it is foreseen that they should be by the time data-taking is complete. There is a significant amount of data and simulation to process, so that even with the invaluable computing resources available through WestGrid, the final results will not be available immediately.

The original goals of TWIST, to improve the precision of all three parameters by at least an order of magnitude, still seems realistic. However, only the analysis

of the 2006 and 2007 data will confirm that.

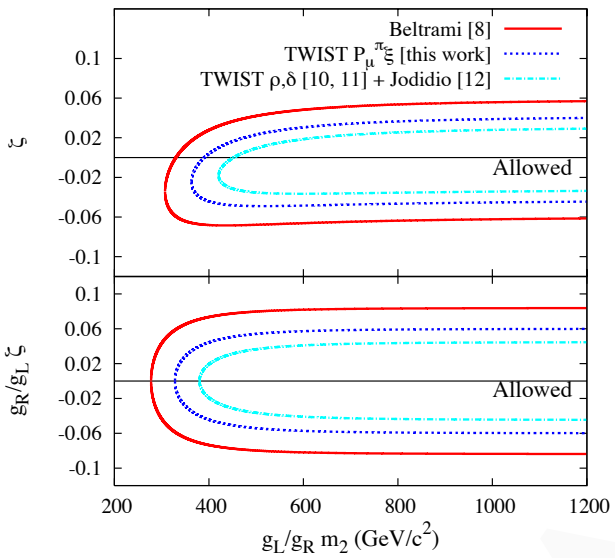

Fig. 1. From Jamieson *et al.* [*op. cit.*], limits on mixing angle vs. mass parameters in a left-right symmetric extension to the standard model, from TWIST and from previous best muon decay determinations.

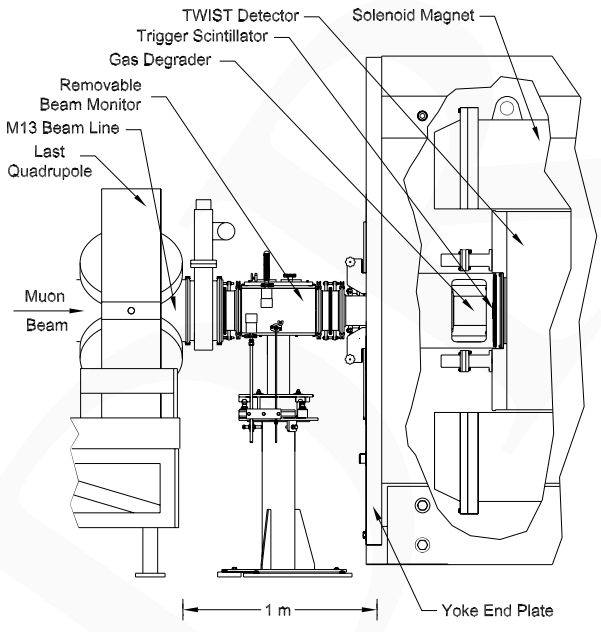

Fig. 2. From Hu *et al.* [*op. cit.*], location of the last beam line quadrupole, beam monitor (TEC), gas degrader, trigger scintillator, and the TWIST solenoid.

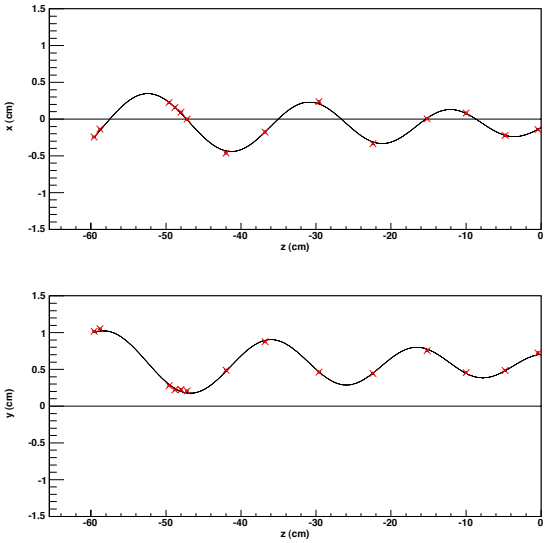

Fig. 3. Mean displacement of the muon beam envelope in the upstream half of the TWIST spectrometer. It shows x and y displacements as a function of distance along the spectrometer axis (z), fit to a damped helix function, for a beam steered away from the magnetic axis.

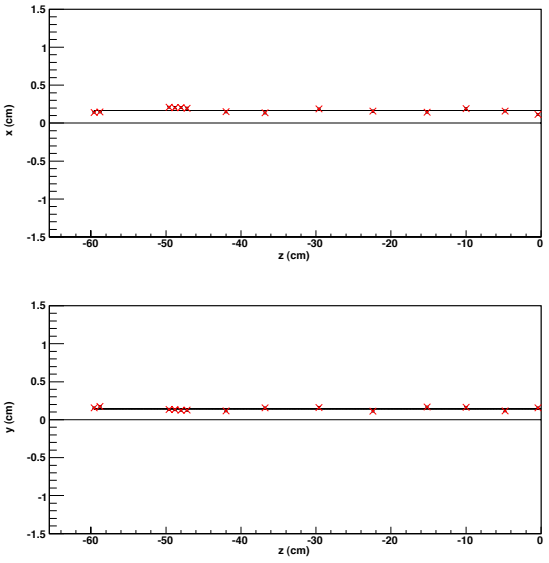

Fig. 4. As in Fig. 3, except that the beam is adjusted to enter along the field direction, on average, to minimize transverse momentum and thus depolarization.

Experiment 1072
PIENU

(D.A. Bryman, T. Numao, UBC/TRIUMF)

Electron-muon universality, the hypothesis that the charged leptons have identical electroweak gauge interactions, has been tested in the context of the standard model (SM) at the 0.16% level by the measurements of the branching ratio of the decays $\pi \to e\nu$ and $\pi \to \mu\nu$, $R_{e/\mu} = \frac{\Gamma(\pi\to e\nu)}{\Gamma(\pi\to\mu\nu)}$. The experimental re-

sults $R_{e/\mu} = (1.2312 \pm 0.0037) \times 10^{-4}$ [Britton *et al.*, Phys. Rev. Lett. **68**, 3000 (1992); Czapek *et al., ibid.* 17 (1993)] are in excellent agreement with the precise SM theoretical predictions [Marciano and Sirlin, Phys. Rev. Lett. **71**, 3692 (1993)] which may be further improved in precision. Because of helicity suppression in the $\pi \to e\nu$ decay, the $R_{e/\mu}$ is extremely sensitive to pseudo-scalar and scalar couplings which arise in many extensions of the SM, such as those with charged Higgs particles, lepto-quarks and SUSY particles [Ramsey-Musolf and Su, hep-ph/0612057; Campbell and Maybury, Nucl. Phys. **B709**, 419 (2005)]. The goal of the new PIENU experiment is to measure the branching ratio with precision improved by a factor of 5 or more to <0.1%.

The time and energy spectra of positrons from the decays $\pi^+ \to e^+\nu$ ($T_{e^+} = 69.3$ MeV) and $\mu^+ \to e^+\nu\bar{\nu}$ ($T_{e^+} = 0$–52.3 MeV) following the decay $\pi^+ \to \mu^+\nu$ ($\pi^+ \to \mu^+ \to e^+$ decay) will be measured using an inorganic-crystal detector array (a 50 cm diameter, 50 cm long NaI crystal with surrounding CsI crystals) covering a solid angle of 25%. Simultaneously fitting the time distributions of $\pi^+ \to e^+\nu$ and $\pi^+ \to \mu^+ \to e^+$ decays provides $R_{e/\mu}$. Small corrections will be applied for $\pi^+ \to e^+\nu(\gamma)$ events below 52 MeV which are hidden under the $\pi^+ \to \mu^+ \to e^+$ spectrum and to account for the effects related to the energy dependence of positron interactions.

In 2006, a feasibility test of the experiment was carried out at the M9A channel. The primary goals included testing beam counters, observing fast and slow pulses with new 500 MHz and 62 MHz digitizer systems, injecting a beam into the TRIUMF NaI crystal (TINA), and studying the effect of absorbers in the beam. Pions at 70–85 MeV/c with momentum bite of 3.5% (FWHM) were stopped at the centre of a small target scintillator. Decay positrons were detected by a scintillator telescope and TINA. About 5×10^4 $\pi^+ \to e^+\nu$ events were accumulated during the test. Initial analysis indicated that the $\pi^+ \to \mu^+ \to e^+$ decay events could be suppressed relative to $\pi^+ \to e^+\nu$ events using timing, total energy in the beam counters and digitized pulse shape information in the target counter at a level consistent with the previous TRIUMF experiment, Expt. 248 [Britton *et al., op. cit.*].

The CsI crystals from Brookhaven National Laboratory (BNL) E949 have been dismounted from the detector and packed for shipment to TRIUMF. Another large NaI detector presently at the BNL light source will also be sent to TRIUMF to replace TINA. PIENU detector construction and assembly is planned for 2007. The experiment will eventually be mounted at the M13 channel after completion of the TWIST experiment.

The ATLAS Experiment at the LHC

(I. Trigger, C. Oram, TRIUMF)

The international ATLAS collaboration is building a general purpose *pp* detector, as described in detail in the 1996 Annual Report, designed to exploit the full discovery potential of the Large Hadron Collider (LHC) at CERN. The TRIUMF group was responsible for the management and engineering of the hadronic endcap (HEC) calorimeters, and the transport of the two 280-tonne endcap cryostats to the ATLAS pit. These detectors are now installed in the experimental cavern and are being cooled to liquid argon temperatures. The front-end electronics have been installed and commissioned, and the liquid argon calorimeters will begin to take cosmic ray data in spring, 2007. Several of the other detector subsystems are already collecting cosmic data in the pit (see Fig. 1).

As we are now preparing for data-taking, recent hires in the TRIUMF ATLAS group have been focused on preparation for analysis of the initial data and on the ATLAS Tier 1 computing centre located at TRIUMF, which is funded by CFI and BCKDF. The Tier 1 centre is discussed elsewhere in this Annual Report.

The ATLAS detector installation in the pit is well advanced. Figure 2 shows two of the "big wheels" of muon chambers. It is instructive to compare this image with the more spectacular one in last year's Annual Report, which gave a much better view of the detector as a whole because it was still possible to see inside. Now, the cavern is taking on its final appearance: we can see only muon chambers.

The installation of the LHC is progressing well, and over 1000 of the 1200 dipole magnets are now in place. Installation of all major magnets should be completed in March. One octant of the LHC is already being cooled down to operating temperature at the beginning of 2007. Although it is only one eighth of the full LHC, it is already the world's largest operating cryogenic installation. The LHC beam pipe ring will be closed by August 31, 2007, so all large detector components must be in position by that date. The first colliding proton beams are expected shortly after that in late 2007, and the first beams at the nominal energy of 7 TeV will collide by mid-2008.

Physics goals

The present theoretical understanding of elementary particles is in the context of the standard model. It is a remarkably successful model, its predictions having been consistently confirmed by experiments for over three decades. Its agreement with experimental results, to enormous accuracy in some cases, makes it arguably the most accurately verified model in science.

Of the many elementary particles contained in the

standard model, only one remains to be discovered: the Higgs boson, a spinless particle which is required by the spontaneous symmetry-breaking mechanism in the electroweak sector. Electroweak symmetry breaking generates the masses of the gauge bosons and also allows the fermions that make up the fundamental matter of the universe to acquire mass. The Higgs is thus related to one of the most fundamental questions of physics: What is the origin of the different particle masses? New direct experimental insight is required to answer this question.

The simplest manifestation of the spontaneous symmetry-breaking mechanism would be the existence of a standard model Higgs boson (H), but many more plausible models predict multiple Higgs particles. For example, in the minimal supersymmetric extension of the standard model (MSSM), there are five Higgs: $H^{\pm}$, h, H and A.

There are good theoretical reasons to believe that the discovery of the Higgs will be accompanied by hints of, and more likely direct evidence for, physics beyond the standard model. In the standard model, which is a highly nonlinear dynamical system, elementary particles tend to take on the heaviest of all possible mass scales, which in such a model are at inaccessible energies and inconsistent with other requirements of the model. All particles discovered thus far have natural mechanisms, such as gauge and chiral symmetries, for protecting their masses so that they can lie in the observable range. For the Higgs particle, there is no such symmetry in the present model.

Theoretical scenarios which leave the Higgs particle light enough to be observed include technicolour, supersymmetry and models invoking extra dimensions in which gravity can propagate with a strength comparable to the nuclear and electromagnetic forces. If a Higgs is observed at the LHC, its mass, spin properties and couplings should begin to elucidate the nature of the physics beyond the standard model. If the Higgs is composite, its existence requires as yet unknown ultrastrong forces. If it is elementary, it would be the first spinless elementary particle ever discovered.

There is a theoretical "naturalness" problem for the masses of spinless particles. The present theoretical view is that the conventional grand unification of the strong, weak and electromagnetic forces can only work in the supersymmetric extension of the standard model. In that model, the grand unified energy scale is only two decades below the Planck scale, the energy at which space-time itself has quantum fluctuations. Models with extra dimensions solve the naturalness problem differently, by postulating that the gravitational and electroweak forces actually have comparable strengths in the full multi-dimensional space-time bulk, but that since gravity propagates in all dimensions and electroweak interactions only on the "brane" containing the four that we know, gravity appears to be much weaker.

The central goal of ATLAS is the search for the Higgs, or Higgs-like particles. Whatever the precise nature of the mechanism by which electroweak symmetry is broken, new particles, including at least one which must play the role of the Higgs, are expected in the TeV-energy region. Experiments at the LHC, where the ATLAS detector will take data, will probe this energy region. This will be the first experimental probe in many years of an energy region where fundamentally new physics is definitely expected to occur. There is every reason to believe that the results will be among the most dramatic ever.

In supersymmetric scenarios, we expect to observe not only Higgs bosons, but also many new supersymmetric partners of the fermions. These typically decay in cascades, ending with a stable lightest supersymmetric particle (LSP) which interacts only weakly with the detector and thus escapes undetected. Supersymmetric signatures therefore consist of jets, leptons and, most crucially, missing transverse energy from the escaping LSP.

Similarly, in models with large extra dimensions, we may expect to find additional massive scalars, as well as tiny black holes. The black holes are formed because gravity is so strong when we include the components propagating in the extra dimensions that the Schwarzschild radius is extremely small and interactions between partons of TeV energy can thus be transplanckian and result in black hole formation. The signature for black hole formation also consists of jets and missing transverse energy.

The observable cross sections for most of these processes are small over a large part of the mass range to be explored at the LHC. Hence it is important to operate at high luminosity, and to maximize the detectable rates above backgrounds by high-resolution measurements of electrons, photons, and muons. Initial analysis design focuses on simple, cut-based selections which will help us to calibrate the jet-energy scale, understand the calorimeter resolutions, and eventually measure missing transverse energy.

The possible signatures of new particles from physics processes beyond the standard model are many and various, which is why ATLAS is such a large and complicated detector. In general, though, most models predict Higgs-like particles which decay to b-quark jets or to photons, requiring an excellent understanding of the calorimeters. Similarly, most supersymmetry-like models, including models with large extra dimensions or technicolour, have signatures involve missing trans-

verse energy, which can only be measured if the jet response and electromagnetic response of the calorimeters are well understood.

From 100–190 GeV/c^2, the most significant discovery channels are those where the Higgs is produced by vector boson fusion [see Asai *et al.*, "Prospects for the search for a standard model Higgs boson in ATLAS using vector boson fusion", ATLAS Note SN-ATLAS-2003-24]. While the production cross section is lower in these channels, the ability to tag the Higgs production cleanly using forward jets that enter the endcap calorimeters more than compensates, yielding superior signal to noise. The need to use the endcap calorimeters for this tag puts a premium on obtaining an early robust calibration for the calorimeters over the entire angular range.

The TRIUMF group is well placed to be in the front lines of the discovery effort: our calorimetry expertise is supplemented by extensive knowledge of many of the other detector subsystems, experience with many other collider experiments, and the computing expertise needed for efficient access to the data. Our new post-doctoral fellow, Arthur Moraes, is an expert on minimum bias and underlying events. His knowledge and experience will be a valuable addition to our early physics analysis efforts. Because a significant portion of the ATLAS hadron calorimeter system was designed and built at TRIUMF, we are making an effort to focus our initial analysis efforts around understanding instrumental fake missing energy and the jet-energy scale (in events consisting of Z bosons and jets) and making sure that there is adequate validation of hadronic reconstruction. We can then move on to studies of topologically similar events consisting of associated production of a Z boson and a Higgs boson decaying to jets. We are also interested in vector boson fusion, simple top quark mass measurements and Higgs production in supersymmetry cascades, all of which fit into this program of calorimeter-intensive studies which can be done with the first few months' data from the LHC. We plan to study cosmic ray events with ATLAS as a summer student project, when the liquid argon endcap calorimeters join in the cosmic run.

We make an ongoing effort to exercise the available computing resources as much as possible, with a view to increasing our local technical expertise. We have tried to centralize local ATLAS software at TRIUMF, to minimize time spent by individual physicists on installing new software releases. We use the LCG GRID resources to access centrally produced Monte Carlo simulated data files and to submit analysis jobs. We also use WestGrid facilities to generate simulated data samples for local use.

The TRIUMF ATLAS physics group is expected to be an analysis resource for other physicists working in Canada. We are therefore making considerable efforts to document how to do analysis in Canada, and to provide a local supplement to the documentation available at CERN, so that a new student or post-doc can begin to be productive in a minimum amount of time. We are also trying, as equipment permits, to set up our resources and analyses in "official" ATLAS ways. Our regular weekly meetings with our colleagues at the universities of Victoria and British Columbia, and Simon Fraser University, where we discuss analysis and commissioning work in progress, have been expanded to include ATLAS members from the universities of Alberta and Regina. We hosted a Canada-wide ATLAS physics analysis meeting at TRIUMF in April, 2006. Isabel Trigger has recently been elected ATLAS-Canada Physics Coordinator for a term of two years, which fits well in the context of these activities.

Canada's participation in ATLAS

The Canadian group consists of about 40 grant-eligible physicists from TRIUMF, University of Alberta, University of British Columbia, Carleton University, McGill University, Université de Montréal, University of Regina, Simon Fraser University, University of Toronto, University of Victoria, and York University. We have been strongly involved in three construction projects centred around detecting hadrons in the endcap region: the hadronic endcap project, the hadronic portion of the forward calorimeter project, and the pipeline electronics for calorimetry. In addition, as part of our common project contribution, we delivered the cryogenic signal feedthroughs for the two liquid argon endcap cryostats. These construction projects are now completed, the calorimeter systems are being commissioned in the ATLAS pit. The cryostats are being cooled down (see Fig. 3) and systems made ready for first beams. TRIUMF is also centrally involved in the detector control system (DCS) for the liquid argon calorimeters, and provides the convener for this project. In ATLAS management Chris Oram is the ATLAS Collaboration Board Chair (see the ATLAS organization chart at http://atlas.web.cern.ch/Atlas/-Management/Organization.gif). He sits *ex-officio* on the ATLAS executive board and is consulted on all major ATLAS appointments.

The hadronic endcap project

The hadronic endcap calorimeter (HEC) is a liquid argon sampling calorimeter with copper absorbers [ATLAS Collab., ATLAS Liquid Argon Technical Design Report (1996)]. A concise overview of this design was provided in the 1996 TRIUMF Annual Report. The construction is now complete, and the detectors

installed in the two endcap cryostats. Four detector systems sit in each endcap cryostat: the presampler is closest to the interaction region and is followed by the electromagnetic endcap calorimeter (EMEC) and the HEC. At the inner diameter, the forward calorimeter (FCAL) is installed around the beam pipe. These calorimeters form the endcap calorimeter system. A paper is in preparation describing the HEC calorimeter and associated systems as installed. We anticipate this will be published in 2007, probably in an open access on-line journal such as the Journal of Instrumentation, in line with the new CERN policy on Open Access publication.

Endcap calorimeter system Both of the 280-tonne endcap calorimeter systems have now been lowered into the ATLAS pit.The emphasis of the work has now shifted to commissioning the equipment in the ATLAS pit.

The detector control system (DCS) The DCS system in the liquid argon calorimeter system covers all aspects of the calorimeter that must be monitored and controlled. These include: the argon purity and temperature, the HV on the calorimeters, and the various voltages on the front-end crates. This system is a responsibility of the TRIUMF ATLAS group, and is functioning now for the detector commissioning.

Test beam measurements of the hadronic endcap at sLHC intensities While we have yet to start taking data with the ATLAS calorimeters, CERN has announced that it intends to push the intensity of the LHC an order of magnitude beyond the nominal maximum LHC intensities in an upgrade that would create a machine called the super LHC (sLHC). The timescale of this upgrade is about 2012. The intensities of the sLHC will create a challenge for the ATLAS endcap liquid argon calorimetry. The forward calorimeter will move into an operational mode, in the forward region, where the charge resident on the plates that form the calorimeter will be less than the positive charge of the ions in the liquid argon between the plates. No calorimeter has been operated in this mode. Predictions of how the calorimeter will operate are hampered by knowledge of such things as the positive ion mobility and the charge recombination rate. Tests are being planned to run test cells in an intense 60 GeV proton beam (10^9 particles per second) to simulate this situation. The TRIUMF group is involved in the specification of these tests, including the required proton beam pulse structure and the design of the mechanical and electronic equipment.

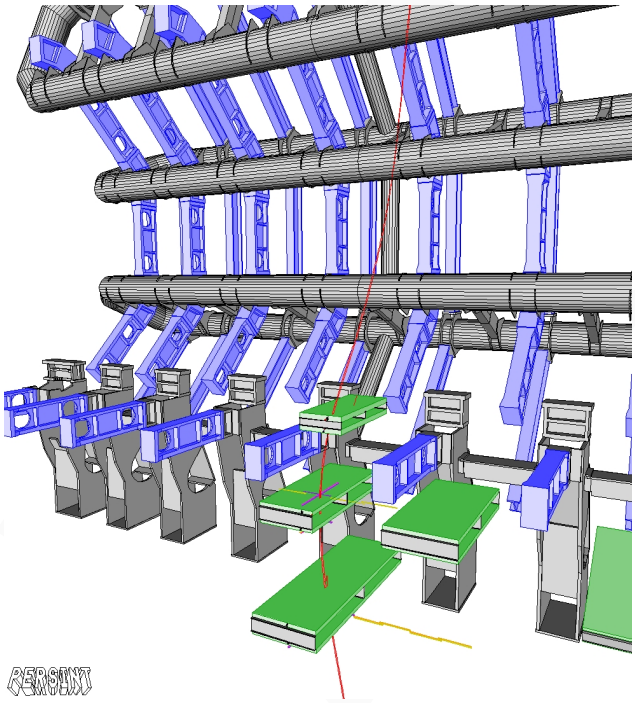

Fig. 1. Cosmic muon in MDT/RPC with toroid on – November, 2006 – run 100372 event 15.

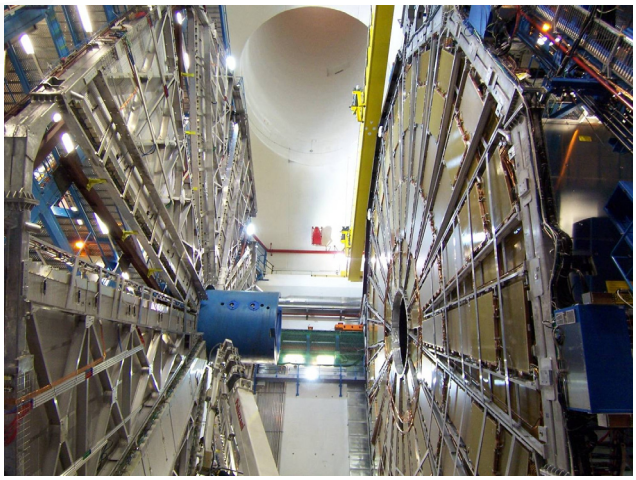

Fig. 2. In contrast with last year's spectacular photograph of the entire detector, this year's view of the cavern shows that ATLAS is now so close to completion that only muon chambers are visible.

Fig. 3. Cryogenic status of the ATLAS liquid argon calorimeters.

K2K

Calibration source manipulator

(R. Helmer, TRIUMF)

As reported in last year's Annual Report, data were taken with the calibration source manipulator at over 200 locations within the detector volume. Preliminary analyses of these data showed a reconstructed position resolution (rms) of 3 cm. This resolution was slightly poorer than the design goal but several arm position corrections were not yet included in the analysis. In any event it was adequate for detecting gross errors in the reconstructed positions.

Before going to a more refined analysis, we also looked at data taken with the laser ball simply hanging on a wire down the central axis of the detector. Using this technique, the distances between laser ball positions could be accurately measured simply by noting the length of the wire. A puzzling result of these measurements was that the reconstructed positions differed significantly (a few cm in 3 m) from the known laser ball position. Unfortunately, the student working on the analysis graduated at this time and also the detector had been decommissioned so no further measurements were possible. With the group's effort now focused on T2K (see elsewhere in this Annual Report), we have not continued with these investigations.

Sudbury Neutrino Observatory

(R. Helmer, TRIUMF)

Collection of neutrino data with SNO came to an end November 28 when the PMTs were powered down. A total of 731 days of data were collected during the final, NCD, phase of the experiment. By the end of the year, removal of the NCDs was under way and plans were being developed for the removal of the heavy water and its return to Ontario Hydro.

Overall, the experiment was a huge success, culminating with the presentation to the collaboration of the NSERC John C. Polanyi Award on November 15. This prize is awarded annually for a recent outstanding advance made by Canadian researchers in any field of the natural sciences or engineering.

TRIUMF's infrastructure role during the year was limited to deployment of the lithium-8 source, for which TRIUMF has operational responsibilities. Data were collected on two separate occasions. A total of 36,000 tagged lithium-8 decay events were collected; analysis of these data is under way.

There was one new paper published during the year – the results of searches for neutrinos from the *hep* reaction in the sun and for a diffuse background of neutrinos from previous supernovas (DSNB neutrinos). Blind analysis procedures were carried out for both searches. In the *hep* search, two events were found in the signal box from 14.3 MeV to 20 MeV effective electron energy, where 3.1 background events were expected. After accounting for neutrino oscillations, an upper limit of 2.3 $\times$ 10^4 cm^{-2}s^{-1} at 90% confidence was inferred on the integral total flux of *hep* neutrinos. For DSNB neutrinos, no events were observed in the signal box from 21 MeV to 35 MeV effective electron energy, leading to an upper limit on the ν_e component of the DSNB flux of 70 cm^{-2}s^{-1} at 90% confidence in the neutrino energy range of 22.9 MeV to 36.9 MeV. These results are improvements by factors of 6.5 (*hep* neutrinos) and two orders of magnitude (DSNB flux) from the previous best upper limits.

TJNAF Experiment E00-006/E04-115/E06-008 Measurement of the flavour singlet form factors of the proton ($G\emptyset$)

(W.T.H. van Oers, Manitoba)

The $G\emptyset$ experiment (TJNAF experiment E00-006/E04-115/E06-008) will measure parity-violating electron scattering from the proton at a range of momentum transfers up to 1 GeV^2 and at forward and backward scattering angles; from these data and additional data at backward scattering angles from the deuteron at the same incident energies, the electric and magnetic weak neutral vector current proton form factors – G_E^Z and G_M^Z – will be determined. While these form factors are of fundamental importance in their own right, the prospect of determining the strange quark contributions to G_E^Z and G_M^Z, which can be accomplished by combining the $G\emptyset$ data with previous electromagnetic measurements of G_E^γ and G_M^γ, is of great current interest. The objective of the $G\emptyset$ experiment is to determine these contributions to the proton form factors at the few per cent level. Very little is known about strange quark contributions to these

form factors, though tantalizing evidence from a host of other experiments indicates that strange quarks may play a nontrivial role in the nucleon structure. The G∅ experiment is very challenging because of the small size of the asymmetries to be measured ($\simeq 5 \times 10^{-6}$) and the high statistical accuracy needed ($\frac{\Delta A}{A} = 5\%$) to achieve adequate sensitivity to the strange quark contributions.

The G∅ experiment has the highest possible priority for execution at Jefferson Lab, and will be the first to probe the proton structure in this detail. It is funded by the U.S. Department of Energy and the U.S. National Science Foundation, by the Natural Sciences and Engineering Research Council of Canada, and by the Centre National de la Recherche Scientifique of France.

The physics of G∅

In the G∅ experiment, a unique approach will be used to gain insight into the consequences of QCD at low energies. The quark-antiquark sea, whose importance at these energies is relatively unknown, is usually subsumed in effective degrees of freedom in theoretical descriptions of hadronic structure, such as constituent quark models and chiral perturbation theory. Because parity-violating electron scattering asymmetries are sensitive to strange quark contributions, they can provide direct information on the importance of the quark-antiquark sea in the nucleon at low energies. It should be noted that establishing even an upper limit on the strange quark contribution of a few per cent (the anticipated level of sensitivity of the G∅ experiment) will be as important as the indications of strange quark contributions of tens of per cent from other, complementary experiments discussed below.

There is experimental evidence suggesting that the strange quark contributions to various hadronic matrix elements may be significant – notably the Ellis-Jaffe sum rule measurements [Adeva *et al.*, Phys. Lett. **B362**, 553 (1993); Anthony *et al.*, Phys. Rev. Lett. **71**, 959 (1993); Ashman *et al.*, Nucl. Phys. **B328**, 1 (1989)] and the pion-nucleon σ term [Donoghue, Ann. Rev. Nucl. Part. Sci. **39**, 1 (1989); Glaser *et al.*, Phys. Lett. **B253**, 252 (1991)]. These measurements determine axial-vector and scalar strange quark current matrix elements in the proton; the related quantity in the G∅ experiment is the weak vector strange quark current matrix element. Not at issue is the presence of strange quarks in the nucleon – deep inelastic scattering data [Abramowicz *et al.*, Z. Phys. **C15**, 19 (1982)] have shown that they could contribute to the nucleon spin at the level of a few per cent – but rather their contributions to various electroweak currents in the proton which have been heretofore unexplored.

The G∅ experiment will measure the parity-violating longitudinal analyzing power in elastic electron-proton scattering at momentum transfers in the range $0.1 \leq Q^2 \leq 1.0$ $(\mathrm{GeV}/c)^2$ at both forward and backward angles. The parity-violating analyzing power depends both on the electromagnetic proton form factors, G_E^γ and G_M^γ, and on the analogous neutral weak current form factors, G_E^Z and G_M^Z, as outlined below.

Electron scattering from current distributions is described by the coherent sum of γ and Z° amplitudes: $\mathcal{M} = \mathcal{M}^\gamma + \mathcal{M}^Z$. The amplitude $\mathcal{M}^Z$ is only 10^{-5} as large as $\mathcal{M}^\gamma$ and is usually neglected. However, the Z° amplitude, unlike $\mathcal{M}^\gamma$, contains both vector and axial-vector terms. Therefore, the cross term in the differential cross section is parity-violating. This cross term can be determined experimentally by measuring the normalized difference of the scattering yields for positive and negative helicity polarized electron beams incident on a target. The longitudinal analyzing power is given by:

$$A_z = (1/P_z)\,\frac{(\sigma^+(\theta) - \sigma^-(\theta))}{(\sigma^+(\theta) + \sigma^-(\theta))} \propto \frac{\mathcal{M}^\gamma \mathcal{M}^Z}{|\mathcal{M}^\gamma|^2}\,,$$

where P_z is the beam polarization and + and − denote the helicity states of the polarized beam. In terms of the form factors defined above, the analyzing power for elastic electron-proton scattering can be written [Napolitano, Phys. Rev. **C43**, 1473 (1991); Musolf *et al.*, Phys. Rep. **239**, 1 (1994)]:

$$A_z = -(1/P_z)\,\frac{G_F Q^2}{\pi\alpha\sqrt{2}}\,\{A_E + A_M + A_A\}/A_D$$

where:

$$\begin{aligned}
A_E &= \epsilon G_E^\gamma G_E^Z\,,\\
A_M &= \tau G_M^\gamma G_M^Z\,,\\
A_A &= -\frac{1}{2}[1 - 4\sin^2(\theta_W)]\sqrt{\tau(1+\tau)(1-\epsilon^2)}\,G_M^\gamma G_A^Z\,,\\
A_D &= \epsilon (G_E^\gamma)^2 + \tau (G_M^\gamma)^2\,,\\
\epsilon &= [1 + 2(1+\tau)\tan^2(\theta/2)]^{-1}\,,\\
\tau &= \frac{Q^2}{4M^2}\,.
\end{aligned}$$

The quantity ϵ can be varied between zero and unity for a fixed Q^2 by varying the incident beam energy and electron scattering angle. The axial-vector term proportional to G_A^Z arises from the axial-vector current in the proton which may couple directly to the Z°. Note that its contribution is suppressed relative to the vector "electric" and "magnetic" terms due to the factor $(1 - 4\sin^2(\theta_W)) \approx 0.07$. Despite this suppression, it is necessary to know the value of G_A^Z in order to deduce G_E^Z and G_M^Z from measurements of A_z; an excellent theoretical discussion is found in Musolf *et al.*

[*op. cit.*]. The recent results from the SAMPLE experiment [Spayde *et al.*, Phys. Rev. Lett. **84**, 1106 (2000)] have pointed to the need to measure G_A^Z in a separate measurement using deuterium as a target.

Given a knowledge of G_A^Z, it is possible to separate the remaining contributions of G_E^Z and G_M^Z to A_z by making measurements at the same momentum transfer but different values of ϵ. (This technique is analogous to the Rosenbluth separation method for ordinary electron scattering.) The magnetic term, A_M, dominates the analyzing power over the range of the experiment. It is therefore not possible to extract information about G_E^Z with forward angle measurements alone. In the extreme backward ($\theta = 180°$) and forward ($\theta = 0°$) angle limits, $\epsilon = 0$ and 1 respectively. For the measurements in the $G\emptyset$ experiment, $\epsilon = 0.95 - 0.99$ for the forward angle measurements and $\epsilon \approx 0.2$ for the backward angle measurements.

Measurements of A_z in polarized electron-proton scattering can be analyzed in a model independent framework. One starts by neglecting the heavier quark (c, t, b) contributions and writing the remaining (u, d, s) quark contributions to the weak neutral current form factors $G_E^{p,Z}$ and $G_M^{p,Z}$, in terms of an SU(3) flavour basis. The electromagnetic form factors can then be written as:

$$G_E^{p,\gamma} = G_E^{3,p} + \frac{1}{\sqrt{3}} G_E^{8,p} \,,$$

where

$$G_E^{3,p} = \frac{1}{2}(G_E^{u,p} - G_E^{d,p})$$

is the ordinary isovector form factor, and

$$G_E^{8,p} = \frac{1}{2\sqrt{3}}(G_E^{u,p} + G_E^{d,p} - 2G_E^{s,p})$$

is the SU(3) octet contribution. In this representation, the weak neutral current form factor can be written in terms of the proton electric form factor as:

$$G_E^{p,Z} = \left(\frac{1}{2} - \sin^2(\theta_W)\right) G_E^{p,\gamma} - \frac{1}{4} G_E^{0,p}$$

where the new form factor

$$G_E^{0,p} = \frac{1}{3}(G_E^{u,p} + G_E^{d,p} + G_E^{s,p})$$

is the flavour singlet proton weak electric form factor. The above expressions also hold for the weak magnetic form factors if the subscript E is replaced everywhere by M.

In the above framework, it is seen that the new information obtained from measurements of $G_E^{p,Z}$ and $G_M^{p,Z}$ consists of the flavour singlet weak proton form factors $G_E^{0,p}$ and $G_M^{0,p}$ – hence the name "$G\emptyset$" for this experiment. The flavour singlet form factors, along with the octet form factors, are sensitive to strange quark contributions.

An alternative approach to interpreting the parity-violating asymmetry data is arrived at by expressing the weak and electromagnetic form factors directly in terms of individual quark current contributions. In this framework, the weak form factors for the proton and neutron are written as the appropriate sums over quark constituents:

$$G_{E/M}^Z = \sum_j \left(\frac{1}{2} T_j^3 - Q_j \sin^2(\theta_W)\right) G_{E/M}^j \,,$$

and the electromagnetic form factors are:

$$G_{E/M}^\gamma = \sum_j Q_j \, G_{E/M}^j$$

where $j = u, d, s$ implies a sum over the light quark flavours, Q_j are the charges, and T_j^3 are the corresponding weak isospin projections for the jth quarks. Assuming charge symmetry for the u and d quark contributions, the strange quark contributions to the proton form factors $G_E^{p,Z}$ and $G_M^{p,Z}$ can be deduced in terms of the electromagnetic form factors for the proton and neutron. The strange quark electric form factor of the proton is then given by:

$$G_E^{s,p} = \left(1 - 4\sin^2(\theta_W)\right) G_E^{p,\gamma} - G_E^{n,\gamma} - 4G_E^{p,Z} \,,$$

with a similar expression for the strange quark proton magnetic form factor, obtained by replacing the subscript E with M.

Until recently very little was known about the nucleon strange quark (or equivalently the flavour singlet) form factors. Only the normalization of the strange quark contribution to the charge form factor is well established: since the proton does not carry a net strangeness, $G_E^{s,p}(Q^2 = 0) = 0$. The normalization of $G_M^{s,p}$ and the Q^2 dependences of either form factor are starting to be constrained by experiment. Preliminary results of an analysis of the BNL E734 $p(\nu, \nu)$ experiment [Ahrens *et al.*, Phys. Rev. **D35**, 785 (1987)] indicate that the G_E^s and G_M^s form factors are small over the range of momentum transfer $0.5 \leq Q^2 \leq 1.0$ GeV^2.

There are currently few theoretical models of the nucleon which could predict any strange quark form factors [Leinweber *et al.*, hep-lat/0601025 (2006)]. The phenomenological model of Jaffe [Phys. Lett. **229B**, 275 (1989)] is apparently in disagreement with the analysis of the BNL E734 neutrino scattering data. Attempts have also been made to consider the contributions of possible kaon admixtures in the nucleon wave function, both in the SU(3) Skyrme model [Park

et al., Phys. Rev. **D43**, 869 (1991)] and in Lambda-kaon admixture models [Musolf *et al., op. cit.*; Cohen *et al.*,University of Maryland preprint 93-217]. These models generally give small results. A cloudy bag model calculation [Hong and Park, Nucl. Phys. **A561**, 525 (1993)] predicts a rather large positive $G_M^s(Q^2 = 0)$ of 0.4 n.m., whereas most of the other models predict comparable negative values. In principle, the parity violating analyzing power A_z is sensitive to deviations of the Standard Model as well as to hadronic structure. However, the effect from possible new physics beyond the Standard Model is expected to be about an order of magnitude smaller than what might be expected from strange quarks at these momentum transfers. A new experiment, specific to the search for new physics beyond the Standard Model, the Q_{weak} experiment, is now being prepared for installation at Jefferson Lab starting in 2008.

The parity violating analyzing power to be measured by $G\emptyset$ depends on three terms, each of which has an associated electroweak radiative correction. The corrections for G_E^Z and G_M^Z may be calculated with good precision; the correction for G_E^Z is several times larger than that for G_M^Z. For example, the calculation of the correction factor for G_E^Z, defined by $G_E^Z(\text{measured}) = G_E^Z(\text{tree})(1 + R_E)$ gives $R_E = -0.33 \pm 0.01$ [Musolf and Holstein, Phys. Lett. **242B**, 461 (1990)]. In contrast, a potential source of difficulty for the interpretation of the $G\emptyset$ experiment lies with the much less certain radiative correction for G_A^Z. This radiative correction is estimated to be $R_A = -0.24 \pm 0.22$, where the uncertainty is only a best estimate. The solution to this problem involves a measurement of quasi-elastic scattering from deuterium at the same Q^2 values in order to determine G_A^Z. The parity-violating analyzing power in quasi-elastic scattering from the deuteron at backward angles emphasizes the G_A term. Such a measurement will allow both G_A^Z and its uncertainty to be determined at a level better than quoted above. In backward angle quasi-elastic scattering from deuterium, the strange quark isoscalar effects enter multiplied by essentially $\mu^p + \mu^n = 0.88$, while the axial form factor enters multiplied by essentially $\mu^p - \mu^n = 4.71$. Therefore, in such a measurement the unknown strange quark effects are suppressed relative to the unknown axial form factor radiative corrections.

Information from related experiments

The SAMPLE experiment at the MIT-Bates Linear Accelerator Laboratory detected backward scattered electrons in large air Čerenkov detectors in 200 MeV elastic *e–p* and quasi-elastic *e–d* scattering. The Čerenkov detectors subtended the laboratory angular range from 130° to 170°, corresponding to a four momentum transfer Q^2 of about 0.1 $(\text{GeV}/c)^2$. The value obtained in *e–p* scattering of $A_z = (-4.92 \pm 0.61 \pm 0.73) \times 10^{-6}$ results in $G_M^s = -0.45 G_A^Z + 0.20 \pm 0.17\,(\text{stat.}) \pm 0.21\,(\text{syst.})$ [Hasty *et al.*, Science **290**, 2117 (2000)]. Taking theoretical estimates for the axial form factor G_A^Z leads to a substantially positive G_M^s. However, combining the above result for A_z with the value obtained in quasi-elastic *e–d* scattering $A_z = (-7.55 \pm 0.70 \pm 0.60) \times 10^{-6}$ [Spayde *et al.*, Phys. Rev. Lett. **84**, 1106 (2000)] results in the following values for G_M^s and the isovector part of G_A^Z:

$$\begin{aligned} G_M^s &= 0.14 \pm 0.29\,(\text{stat.}) \pm 0.31\,(\text{syst.}) \\ G_A^Z(T=1) &= 0.22 \pm 0.45\,(\text{stat.}) \pm 0.39\,(\text{syst.})\,. \end{aligned}$$

Consequently the isoscalar and isovector axial radiative corrections, R_A^0 and R_A^1, used in obtaining the theoretical estimate for G_A^Z may be in error. It is to be noted that the isovector radiative correction has a connection to hadronic parity violation (the weak meson-nucleon coupling constants). The HAPPEX experiment at Jefferson Lab detected forward scattered electrons in the two Hall-A HRS spectrometers placed left and right of the incident beam at 12.5°, corresponding to a Q^2 of 0.48 $(\text{GeV}/c)^2$ in 3.335 GeV elastic electron scattering. The latter of the two data-taking runs used strained GaAs crystals to give an electron beam with about 70% polarization. The experiment measured the combination $G_E^s + 0.39 G_M^s$. The result from the first data-taking run is $A_z = (-14.5 \pm 2.0 \pm 1.1) \times 10^{-6}$, which gives:

$$\begin{aligned} G_E^s + 0.39 G_M^s &= 0.023 \pm 0.034\,(\text{stat.}) \pm 0.022\,(\text{syst.}) \\ &\quad \pm 0.026(\delta G_E^n) \end{aligned}$$

[Aniol *et al.*, Phys. Rev. Lett. **82**, 1096 (1999)]. The result of the second data-taking run is $A_z = (-14.60 \pm 0.94\,(\text{stat.}) \pm 0.54\,(\text{syst.})) \times 10^{-6}$ [Aniol *et al.*, Phys. Lett. **B509**, 211 (2001)], in excellent agreement with the result of the first data-taking run. The A4 experiment at MAMI detected forward scattered electrons in 885 MeV parity violating *e–p* scattering at 35° in a cylindrical calorimeter made of 1022 PbF_2 crystals. The experiment has determined a linear combination of $G_E^s + 0.22 G_M^s$ at a Q^2 value of 0.23 $(\text{GeV}/c)^2$ [Maas *et al.* in *Parity Violation in Atoms and Polarized Electron Scattering*, eds. B. Frois and M.A. Bouchiat (1999)].

There are three other experiments of relevance at Jefferson Lab. In experiment E91-004, the longitudinal analyzing power in electron-^{4}He scattering will be measured at a Q^2 of about 0.6 GeV^2. This is a very interesting region, since the original model of Jaffe [*op. cit.*] implies that the strange quark contributions should be

large enough to change the sign of the parity violating analyzing power for ^{4}He as compared to the up and down quark contributions. A measurement with a precision of about 30% in A_z is planned. The analyzing power in this case is sensitive only to the neutral weak current analog of the charge form factor for ^{4}He, because the spin and isospin are both zero. It will be most interesting to compare the results for ^{4}He with those for the proton. In the HAPPEX II experiment, E99-115, the two Hall-A spectrometers have been augmented with septum magnets to reach forward angles of 6°. The longitudinal analyzing power has been measured at 6°, scattering 3.03 GeV electrons from hydrogen, corresponding to a Q^2 value of 0.099 (GeV/c)^2 [Aniol *et al.*, nucl-ex/0506011 (2006)]. The measurement accesses the linear combination $\rho_s + \mu_p \mu_s$ to an accuracy of ± 0.3 and provides an important direct constraint on the nucleon strangeness radius. Using a similar experimental arrangement experiment E00-114 has measured the longitudinal analyzing power in 3.03 GeV electron-^{4}He scattering at 6° corresponding to an average Q^2 of about 0.091 (GeV/c)^2 [Aniol *et al.*, Phys. Rev. Lett. **96**, 022033 (2006)]. This latter experiment measured the leading strange charge coefficient ρ_s to an accuracy of ± 0.05. Combining the ^{4}He measurements with the results from the HAPPEX II experiment (as well as the world data at $Q^2 = 0.1$ (GeV/c)^2) [Paschke, private communication (2006)] yielded the following values:

$$\begin{aligned} G_M^s &= 0.28 \pm 0.20 \\ G_E^s &= -0.006 \pm 0.016\,. \end{aligned}$$

Overview of the $G\emptyset$ experiment

The objective of the $G\emptyset$ experiment is to separate G_E^s, G_M^s, and G_A^Z for two values of Q^2: 0.23 and 0.63 (GeV/c)^2. Making pairs of measurements at forward and backward angles (at backward angles also in quasi-elastic electron-deuteron scattering) with the same apparatus will allow this separation of G_E^Z, G_M^Z and G_A^Z. Predicted longitudinal analyzing powers (with no strange quark contributions) range from about –3 to -40×10^{-6}; it is planned to measure the longitudinal analyzing powers with statistical uncertainties of $\Delta A/A = 5\%$ and systematic uncertainties related to helicity correlated effects of $\Delta A \leq 2.5 \times 10^{-7}$.

In the first phase of the experiment, longitudinal analyzing powers have been measured simultaneously for momentum transfers in the range $0.1 \leq Q^2 \leq 1.0$ (GeV/c)^2. In the second phase of the experiment, each subsequent backward angle analyzing power measurement would require approximately 700 hours of running time. It should be noted that the overall uncertainties quoted for the recent parity violation experiments at Jefferson Laboratory (the HAPPEX experiments) as well as the results obtained in the $G\emptyset$ commissioning run indicate that systematic uncertainties of a few times 10^{-7} should be attainable. As noted, the second phase of the experiment will also include quasi-elastic scattering measurements from deuterium to access the axial form factor G_A^Z.

Experimental details

To achieve the desired precision in a reasonable amount of time, the experiment must be performed at high luminosity and with a large acceptance detector. The spectrometer provides the unique capability of measuring both the forward and backward angle analyzing powers. In the first (forward angle) phase of the experiment, elastically scattered recoil protons, with $320 \leq p' \leq 797$ MeV/c and $77.4° \geq \theta' \geq 61.2°$, were detected in order to avoid having to detect electrons at very forward scattering angles; the incident electron beam energy was 3.0 GeV. The solid angle acceptance for the forward angle measurement ranged from 0.20 to 0.11 sr. Secondly, for the backward angle analyzing powers, the spectrometer has been turned around by 180° in order to detect electrons at the corresponding angle centred at about 110° with a solid angle acceptance of 0.9 sr at $Q^2 = 0.2$ (GeV/c)^2 to 0.5 sr at $Q^2 = 1$ (GeV/c)^2. The incident beam energies for the backward angle measurements will be 0.36 ($Q^2 = 0.23$ (GeV/c)^2), and 0.69 GeV ($Q^2 = 0.63$ (GeV/c)^2).

The spectrometer consists of a toroidal array of eight superconducting coils with a field integral of approximately 1.6 Tm. The spectrometer is designed to focus particles of the same momentum and scattering angle from the length of the extended target to a single point, with zero magnification in the dispersion direction. The bend angle of about 35° at the highest momentum is sufficient to allow complete shielding of the detectors. Individual particle detection is used rather than integral counting techniques. Individual particle detection provides the possibility of using time-of-flight (forward angle) or trajectory discrimination (backward angle) to supplement the resolution of the spectrometer. For the forward angle measurements, time-of-flight techniques require a pulsed beam (31.25 MHz), whereas the backward angle measurements make use of the regular CW beam (499 MHz).

The $G\emptyset$ spectrometer has a number of advantages for this electron-proton parity violation experiment. It has very large solid angle and momentum acceptance. The solid angle acceptance has axial symmetry, as does the LH_2 target, which reduces the sensitivity to a certain class of systematic errors. The shape of the magnetic field is determined by the current conductors; there is no polarized iron in the target and spectrometer, and the magnetic field at the spectrometer symmetry axis, which is to coincide with the tar-

get symmetry axis and beam axis, is zero. Both forward and backward angle analyzing powers can be measured with minimal changes in the instrumentation. The $G\emptyset$ spectrometer is a stand-alone device which can coexist with the Hall C Conceptual Design Report instrumentation, thereby providing the stability of a set-up required for measurements of small asymmetries. The $G\emptyset$ spectrometer is of a relatively simple design and has performed exceptionally well during the commissioning run.

Various types of backgrounds have been investigated for both forward and backward angle measurements. For the backward angle measurements, where electrons are detected, the π^- background is kinematically forbidden for the proton target and low incident energies. However, there is a π^- background from the various windows of the target which requires consideration. Inelastically scattered electrons are adequately separated from the electrons of interest. For the deuterium target the π^- background requires the introduction of Čerenkov aerogel detectors in order to suppress this background.

The data-taking pattern is chosen to reduce random background noise. The standard measurement interval will be 1/30 s, i.e., the beam helicity will be reversed at a frequency of ∼30 Hz, with short intervals between measurements to reverse helicity and read out the spectrometer and monitoring equipment. The helicity pattern $+--+$ and its complement will be randomly chosen to further reduce background noise.

The liquid hydrogen target has a length of 0.20 m. With a 60 μA average beam current, the total power deposited by the beam will be about 370 W. The beam is scanned over a target area of about 0.2 cm^2. The position sensitivity of the apparatus near the geometrical neutral axis is small enough to allow scanning over the 0.2 cm^2 target area.

Precise monitoring and control of the incident beam properties is required for the experiment. For each measurement interval the beam properties – position, angle, size, energy, polarization, and charge – are measured. Based on the present design of the experiment, position measurements with a precision of 25 μm will be required for each measurement interval; the most stringent requirements are for the position measurements used to determine the beam energy centroid. During the experiment, continuous monitoring of false asymmetries due to changing beam properties requires substantial interaction (some in the form of feedback loops) with various accelerator and beam transport magnet controls.

The $G\emptyset$ collaboration

The $G\emptyset$ experiment is being carried out by a collaboration of approximately 60 researchers from Canadian, French, and US institutions, and brings together much expertise in both electron and proton parity violation experiments. The Canadian subgroup consists of researchers from the Universities of Manitoba, Northern British Columbia and Winnipeg, and from TRIUMF. Of particular significance is the leadership role played by the University of Manitoba group in the proton-proton parity violation experiment at TRIUMF, where precisions were achieved more than a factor of ten higher than required in the $G\emptyset$ experiment. The Canadian subgroup has successfully carried out a series of very challenging symmetry tests over a time span of some 25 years. With the group's substantial size and proven expertise, it is having a considerable impact on the construction and execution of the $G\emptyset$ experiment.

Canadian contributions

The Canadian members of the $G\emptyset$ collaboration, based at the Universities of Manitoba, Northern British Columbia, Winnipeg, and TRIUMF, have made the following contributions:

1. Designed and produced specialized photomultiplier tube bases for the focal plane detectors;
2. Designed and fabricated an automated magnetic field mapper complete with its own DAQ (this device will next be used in qualifying and quantifying the magnetic field of the eightfold azimuthally symmetric resistive toroidal magnet for the Q_{weak} experiment);
3. Prototyped and produced the cryostat-exit detectors for the backward angle measurements;
4. Prototyped and fabricated (together with the Grenoble group) the aerogel Čerenkov detectors for background rejection in the backward angle measurements;
5. Designed the support structure for the aerogel Čerenkov and cryostat-exit-detector arrays;
6. Coordinated the implementation of TJNAF-built specialized beam monitors and control apparatus with TRIUMF-built "parity-type" electronics;
7. Designed, purchased and installed additional electronics for the Čerenkov detectors to allow data-taking in multiple experiment mode;
8. Coordinated and scheduled resources for $G\emptyset$ commissioning, engineering, and data-taking runs at TJNAF.

The design, construction and installation of the various subsystems listed above has been completed and all are now operational.

Photomultiplier tube bases The heart of the $G\emptyset$ detection system is a spectrometer which consists of an

eight-sector toroidal magnet, with an array of scintillation detectors, located at the focal surface of each sector. Since data are not acquired in event-by-event mode in this experiment, and the focal plane detectors (FPDs) are the only detectors to measure the scattered particles in the forward angle mode, the performance of these FPDs is of critical importance. The timing and pulseshape characteristics of this system had to be fine-tuned at the hardware level since individual events are not reconstructed. Furthermore, the rates associated with many of the FPD elements are quite high (>1 MHz) and the photon yield(s) spans a large dynamic range. This required a custom-designed divider/base for the photomultiplier tubes. In all, some 300 plus photomultipliers and tube bases (designed and constructed at TRIUMF) have been installed on the $G\emptyset$ detector system, successfully operated during the forward angle phase, and are being used for the backward angle phase.

Magnetic field measuring device An automated field measuring apparatus has been used to provide a magnetic verification of the $G\emptyset$ superconducting toroid (albeit at the low current of 1400 A due to the original construction faults of the magnet) by determining the locations of a pre-specified set of magnetic "reference points". These reference points correspond to the zero-crossing locations of specific field components at selected points of symmetry around the toroidal magnet. The measurement has been carried out by scanning a predefined set of "contour" lines, and determining where specific field components reverse signs. The system is capable of providing a position determination of ± 0.2 mm and a field determination of ± 0.2 G. The device consists of a programmable gantry with full 3D motion anywhere within a 4 m $\times$ 4 m $\times$ 2 m volume, and a set of high precision Hall probes is mounted at the end of a probe boom on the gantry. This device will be reused in the Q_{weak} experiment for verifying and quantifying the magnetic field of the resistive toroidal magnet, QTOR.

Cryostat-exit detectors For the backward angle second phase of the $G\emptyset$ experiment, the addition of a second array of scintillation detectors, located near the spectrometer-cryostat exit windows, is required in order to separate the elastic and inelastically scattered electrons. The geometry of these cryostat-exit-detector (CED) arrays (see Fig. 1) was studied in detail and a reference design was produced by the $G\emptyset$ simulation group. With the resident expertise at TRIUMF in producing high quality scintillation detectors and lightguides, the Canadian subgroup played the lead role in the prototyping and production of the CEDs. A set of prototype CEDs was built at TRIUMF and delivered to the $G\emptyset$ collaboration for studies with cosmic rays. Results from these studies showed that the reference design and the prototype detectors met the specification requirements for these arrays and construction of the "production" CED arrays began at TRIUMF. Fabrication of the CED scintillators for all 8 octants was completed and delivery was made to TJNAF, and fabrication of special helical-bend lightguides began in 2002. In order to achieve the unique helical bend required in the $G\emptyset$ backangle geometry, customized bending jigs were designed and constructed at TRIUMF and tested on a first set of prototype CED lightguides. Production of a full set of lightguides for the first CED octant was completed with delivery to TJNAF in 2003, where they underwent further tests. Production of the lightguides for all 8 octants was completed with delivery to TJNAF in early 2004. The CEDs also make use of the same types of photomultiplier tubes and specialized TRIUMF divider/bases as the focal plane detectors.

Aerogel Čerenkov detectors Monte Carlo simulation results showed that backgrounds from negative pions will be problematic for the backward angle measurements involving the deuterium target. The $G\emptyset$ simulation subgroup focused on characterizing this π^- background and provided options for the design of an additional set of pion-rejection detectors. The $G\emptyset$ Canadian and French (Grenoble) subgroups were asked to jointly undertake the prototyping and construction of this crucial set of detectors, which is made up of an array of aerogel Čerenkov counters. A first set of prototype detectors, using "borrowed" aerogel samples, was constructed in 2001 and tested in the TRIUMF pion beam (M11) in late 2001 and 2002. In 2003, the sample aerogel in the prototype detector was replaced by a first batch of "production" aerogel, and the photon yield (and detector efficiencies) immediately improved. Average yields of approximately 12, 8, and 6 photoelectrons were observed for measurements made at the near, centre, and far ends of the Čerenkov diffusion box (positions were defined relative to the Čerenkov PMT positions). Based on the results with the first prototype detector, a second iteration prototype was designed and became the production version of the Čerenkov detector (see Fig. 2). Construction of four Canadian Čerenkov detectors (there are also four French Čerenkov detectors) was completed by the fall, 2004 and three of the detectors were delivered to TJNAF. The fourth detector remained at TRIUMF for further in-beam tests, carried out in 2004 and early 2005, using the M11 muon/pion beam line. Figures 3 and 4 show the electron efficiencies and the pion-rejection factors for the production detectors, respectively. The fourth Canadian Čerenkov detector was delivered to TJNAF in the summer, 2005.

Backangle support structure Considerable effort went into the engineering design of a support structure for the $G\emptyset$ Čerenkov and CED arrays. Although the Canadian subgroup was initially responsible only for the design of the Čerenkov support structure, it was soon realized that the CED support structure would be closely coupled to the former due to the physical proximity of the two detector subsystems. As such, it was later decided than an integrated design for the two detector subsystems should be pursued. The support structure centres around the use of prefabricated aluminum extrusions from Bosch because of their strength, versatility, and relatively low costs. A series of detailed finite-element analysis studies was carried out at TRIUMF, using the program ANSYS, to identify potential problems and to optimize the strength and cost of the support structure. The design consists of a second Ferris wheel type support structure (the mini-Ferris wheel), which couples to the existing detector support structure (also a Ferris wheel type design) and to linear rails on the existing $G\emptyset$ detector platform. A conceptual illustration of the $G\emptyset$ backward angle configuration is shown in Fig. 5, with the superconducting magnet, the 3 detector arrays (FPD, CED, Čerenkov) in each of the 8 sectors, and their respective support structures. Assembly of all eight backangle detector support octants was completed in late fall, 2004 at TJNAF.

Beam line monitors The success of the $G\emptyset$ experiment will be closely linked to the precise measurement and control of the electron beam properties. To make the subtle, refined asymmetry measurement of 1 ppm or better, the beam properties must be held within tight limits. In pursuit of this, the beam position must be measured to better than 25 μ within a 33 ms time window and the beam current to 40 ppm during the same 33 ms time window. To accomplish this the $G\emptyset$ experiment uses two sets of "XYQ" microwave cavity monitors. These require precision electronics designed and built by TJNAF and by TRIUMF. Specifically, the position monitors produce a voltage signal based on position in the X and Y cavities, and a current proportional voltage signal of the current cavity. The voltage is amplified by dedicated custom built amplifiers. The output from these amplifiers is fed into the TRIUMF precision voltage to frequency converters and thence into the DAQ scalers. One set of these XYQ cavities is installed approximately 30 m upstream of the $G\emptyset$ target. The second set of XYQ cavity monitors is installed on the $G\emptyset$ diagnostic girder immediately before the $G\emptyset$ target. Also on this girder are a pair of standard stripline beam position monitors, a pair of super-harp wire scanners, and an optical transmission viewer. The combination of these monitors will allow a beam position measurement of better than 10 μm per helicity window and an angle measurement of better than 0.5 μrad. Upstream along the beam line there are three additional sets of XYQ monitors. In addition to measuring and tightly controlling the beam properties, there will also be a need to determine the false asymmetries contributed by the beam parameters of position, angle, and current on the target. Knowledge of the false asymmetries is required in order to extract the physics asymmetries and associated uncertainties. The false asymmetries are given by

$$\mathrm{A_f} = \sum \frac{\partial Y}{\partial X_i} \Delta X_i$$

where ∂Y is the change in the detector yield, ∂X_i is the change in the ith beam parameter, and ΔX_i is the helicity correlated asymmetry per quartet. To calculate these false asymmetries, the sensitivities $\partial Y/\partial X_i$ must be measured. This is accomplished by deliberate and controlled beam modulations introduced by sending a dc current to beam steering magnets far upstream of the $G\emptyset$ target. The steering magnet positions are chosen to minimize $x-y$ coupled motion at the $G\emptyset$ target. The slopes $\partial Y/\partial X_i$ will be measured at the beginning of each data-taking run while the helicity asymmetry is measured continuously throughout the run. This modulation system was developed by members of the Canadian subgroup; it was used throughout the forward angle phase and worked as expected. It will again be used during the backward angle running.

Additional electronics for the backward angle measurements Lessons learned from the forward angle phase of the experiment led to a significant redesign of the electronics for the backward angle run. In the forward angle run, time-of-flight was used to distinguish elastically scattered protons from pions and inelastically scattered protons. The "start" for the time-of-flight measurement was a signal delivered by the arrival of beam at an rf cavity close to the target. This necessitated the use of an electron beam pulsed at 31 MHz. The usual Jefferson Lab beam structure is 499 MHz ("continuous beam"), so only one in sixteen rf buckets was filled in order to achieve 31 MHz. However, a small amount of beam always occupies every available bucket. This beam arises from simultaneously running continuous beams for the two other experimental halls. This resulted in false asymmetries from so-called "leakage beam". Fortunately, normally unpopulated regions of the time-of-flight spectrum could be used to correct for the effects of the leakage beam. Originally, the backward angle measurements would also have used 31 MHz beam, in order to reuse electronics from the forward angle experiment. However, owing to the leakage beam asymmetries encountered

in the forward angle experiment, continuous beam will be used for the backward angle mode. The backward angle experiments do not use the time-of-flight technique for particle identification purposes, instead relying on the Čerenkov counters. The use of continuous beam is therefore feasible and necessary, due to the lack of ability to use the forward angle correction scheme. The result of this change is that the experiment must provide its own trigger signals, and additional electronics are required. New front-end electronics were required to make use of the Canadian Čerenkov counters in a way consistent with the new trigger scheme for the experiment. The electronics in question are crucial for trigger generation, for on-line calibration of the Čerenkov counters, and for pion contamination studies. The electronics are also necessary to give sufficient flexibility to have the Čerenkov signals arrive in time with signals from the other detectors used in the experiment (scintillation counters with faster time-response). The final electronics design studies were concluded in spring, 2005. The new electronics purchased over summer, 2005 were two VME leading-edge discriminators, and four VME analogue sum/splitter modules. These electronic modules were installed and tested over the summer and fall, 2005, and custom code was developed to operate them in the experiment.

The $G\emptyset$ forward angle run

The $G\emptyset$ experiment ran in forward angle mode from December 1, 2003 to May 9, 2004. The analysis was completed and the data were unblinded on April 15, 2005 at a $G\emptyset$ collaboration meeting at Jefferson Lab. The final results were officially released at a Jefferson Lab seminar on June 17, 2005. At the same time, the paper was submitted to Physical Review Letters and a preprint (nucl-ex/0506021) was posted to the Cornell arXiv server. In August, the article appeared in Physical Review Letters [Armstrong *et al.*, Phys. Rev. Lett. **95**, 092001 (2005)]. This paper was chosen to be featured in Physical Review Focus (focus.aps.org). The $G\emptyset$ experiment was also featured in the popular press, for example, in the September 3–9, 2005 edition of The Economist [**376**, 72 (2005)].

The data on which the forward angle results are based were taken during 13 weeks of production running from February 9 to May 9, 2004. University of Manitoba personnel staffed a total of approximately 30 person-weeks of shifts. The experiment accumulated approximately 10 Tbyte of good production data corresponding to 701 hr of beam at 40 μA (101 coulombs) on the liquid hydrogen target.

Principle of the experiment An overview of the $G\emptyset$ equipment (forward angle configuration) is shown in Fig. 6. The 3 GeV electron beam enters from the lower right where it first encounters the $G\emptyset$ beam monitors. Continuing from right to left, one sees the liquid hydrogen target service module, the eight-sector superconducting magnet system (SMS), and the focal plane detectors mounted in the eight sector Ferris wheel structure between the SMS and the green wall. Longitudinally polarized electrons scatter from the liquid hydrogen target, and the spectrometer accepts recoil protons in the angular range 62° to 78° (corresponding to 15° to 5° electrons). The principle of the forward angle measurement is shown schematically in Fig. 7. The spectrometer magnet is designed so that protons corresponding to a given momentum transfer (Q^2) are directed to a specific focal plane detector regardless of where in the target they originate. Q^2 from 0.16 to 1.0 $(\mathrm{GeV}/c)^2$ can be measured with one magnet setting. The experiment uses a beam time structure with beam bunches 32 ns apart. This is 16 times the usual Jefferson Lab bunch spacing of 2 ns, and permits the protons from elastic scattering to be separated by time of flight from pions and inelastic protons.

Leakage beam measurement An unanticipated problem was the leakage of beam from the Hall A and B lasers. Hall A and B beams are 499 MHz, but the Hall C beam is 31 MHz. Unfortunately, the beam current monitors which are used to measure the charge asymmetry measure all the time and respond to the total A+B+C beam, whereas the $G\emptyset$ time of flight cut sees only the 31 MHz beam. This means that the correction for charge asymmetry was not right. We were able to measure the effect by looking in a "forbidden region" of the TOF spectrum where the signal could not come from the $G\emptyset$ beam bursts spaced at 32 ms. The leakage was typically 50 nA (c.f. 40 μA Hall C) with 340 ppm charge asymmetry. Corrections were made for the effects of beam leakage. The leakage correction is estimated to contribute $\sim$0.14 ppm systematic uncertainty.

Helicity correlated beam properties The helicity of the longitudinally polarized electron beam was selected every 1/30 second. The spin states were chosen in quartets, either $+--+$ or $-++-$, the first state of the quartet being chosen at random. Ideally, no other beam property would be affected, but in practice small changes in beam properties other than helicity occur. Thanks to good design practices such as cylindrical symmetry, the sensitivity of the experiment to helicity correlated beam properties was very small. Nevertheless, it was necessary to constantly monitor helicity correlated beam properties and to correct for the resultant false asymmetry. Table I shows the helicity correlated beam parameters for the forward angle data. Charge and position feedback were used. The helicity correlated beam properties are all very small

and, taken together, only produced a false asymmetry of ∼0.02 ppm.

Correction for background The measured asymmetry is a weighted sum of the true elastic asymmetry and the asymmetry of the background:

$$A_{\rm meas} = f_{\rm el}A_{\rm el} + f_{\rm back}A_{\rm back}\,.$$

To correct for the background, we must know both the background fraction, $f_{\rm back}$, and the asymmetry, $A_{\rm back}$, under the elastic peak. Figure 8 illustrates how these numbers were determined. We first fit the yield spectrum with a Gaussian peak plus a fourth order polynomial background and extracted the background fraction. We then fit the asymmetry spectrum with a second order polynomial and extracted the asymmetry of the background under the elastic peak. We tried several different, but reasonable, fitting methods and used the variation in results to assign a systematic uncertainty to the background correction, which was the dominant source of systematic error. This and the other sources of systematic error are summarized in Table II.

Final results The final analyzing powers obtained by the $G\emptyset$ forward angle run after all corrections are plotted as a function of Q^2 are shown in Fig. 9. The inner error bars are statistical only, whereas the outer error bars are statistical plus systematic errors that affect only that point. Global systematic errors that would affect more than one point in a correlated way are shown by the grey band. The solid curve is the asymmetry expected for "no vector strange". It is calculated using the parameterization of Kelly [Phys. Rev. **C70**, 068202 (2004)] for G_E and G_M and assuming that G_E^s and G_M^s are zero. Since the data shown on Fig. 9 are taken at forward angles only, they determine a linear combination of G_E^s and G_M^s.

The $G\emptyset$ backward angle run

After completion of the $G\emptyset$ forward angle runs in 2004, the superconducting toroidal magnet and the detector system was rotated around a vertical axis (centred at the $G\emptyset$ target) by 180° and readied for installation of additional backward angle detectors (i.e. the Čerenkov and cryostat-exit detectors).

In April, 2005, *in-situ* assembly of all cryostat-exit detectors, on their respective mini-Ferris wheel (support) octants, was completed. Following this, in July, 2005, mounting of all Čerenkov detectors onto their respective mini-Ferris wheel octants was completed. During this period, an octant lifting and rotation jig, designed at TJNAF for lifting, rotating, and positioning each backangle octant onto the main $G\emptyset$ detector Ferris wheel, was assembled at Jefferson Lab's EEL cleanroom and prepared for an initial set of rotation tests. These rotation tests were carried out in July, 2005, and a 360° rotation was successfully completed for one backangle octant. As part of the rotation test procedure, the octant was held upside down overnight for the purpose of a prolonged stress test (see Fig. 10).

In early November, 2005, the 8 fully-assembled detector octants were moved from the EEL cleanroom at TJNAF into Hall C. They were then installed, one octant at a time, onto the existing detector support structure, to form the front-end mini-Ferris wheel subsystem (see Fig. 11).

Beam time for the backward angle commissioning run and a first short production-data run (Run I) took place from March 13 to May 18, 2006. During this period, all of the backward angle subsystems (beam, magnet, cryogenic targets, detectors, electronics, and DAQ) were successfully turned on and operated. This was followed by 2 cycles of full production-data runs (Run II, 362 MeV beam on the liquid hydrogen target) from July 18 to September 2 and (Run III, 687 MeV beam on the liquid hydrogen target and a partial data set on the liquid deuterium target) from September 21 to December 22.

Future Further production-data runs are scheduled for 2007 (Run IV and Run V).

Canadian subgroup of the $G\emptyset$ collaboration: J. Birchall, A. Coppens, W.R. Falk, M. Gericke, L. Lee, S.A. Page, W.D. Ramsay, W.T.H. van Oers (Manitoba); E. Korkmaz, T. Porcelli (Northern British Columbia); J.W. Martin (Winnipeg); C.A. Davis (TRIUMF).

Table I. Helicity correlated beam properties for the forward angle production run compared to $G\emptyset$ specifications. These must be multiplied by the sensitivity to these quantities to give the false signal.

Beam parameter	Achieved	Specification
Charge asymmetry	-0.14 ± 0.32 ppm	1 ppm
x position difference	3 ± 4 nm	20 nm
y position difference	4 ± 4 nm	20 nm
x angle difference	1 ± 1 nrad	2 nrad
y angle difference	1.5 ± 1 nrad	2 nrad
Energy difference	29 ± 4 eV	75 eV

Table II. Sources of systematic error. The table shows the source of the error, the correction made for the error, and the uncertainty introduced by making the correction.

Source	Correction	Uncertainty
Deadtime	0.05 ppm	0.05 ppm
Helicity-correlated beam properties	0.02 ppm	0.01 ppm
Leakage beam	0.71 ppm	0.14 ppm
Beam polarization	73.7%	1%
Background	–1 to +42 ppm	0.2 to 9 ppm

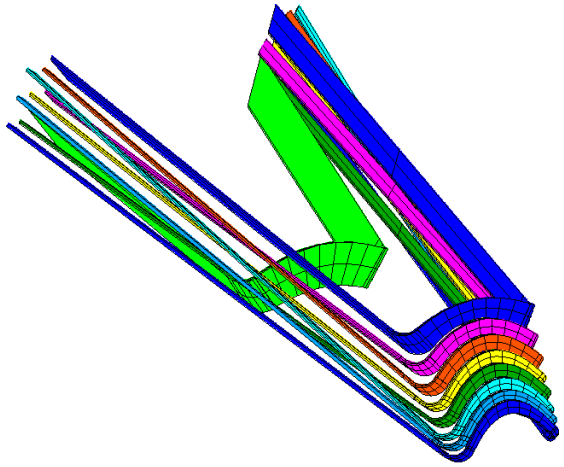

Fig. 1. Layout of a cryostat-exit detector (CED) array for a single octant.

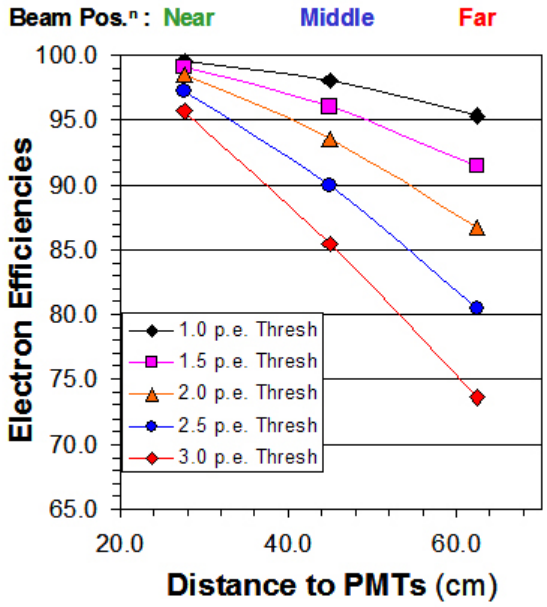

Fig. 3 The position-dependent efficiencies of the aerogel Čerenkov detector for various threshold settings.

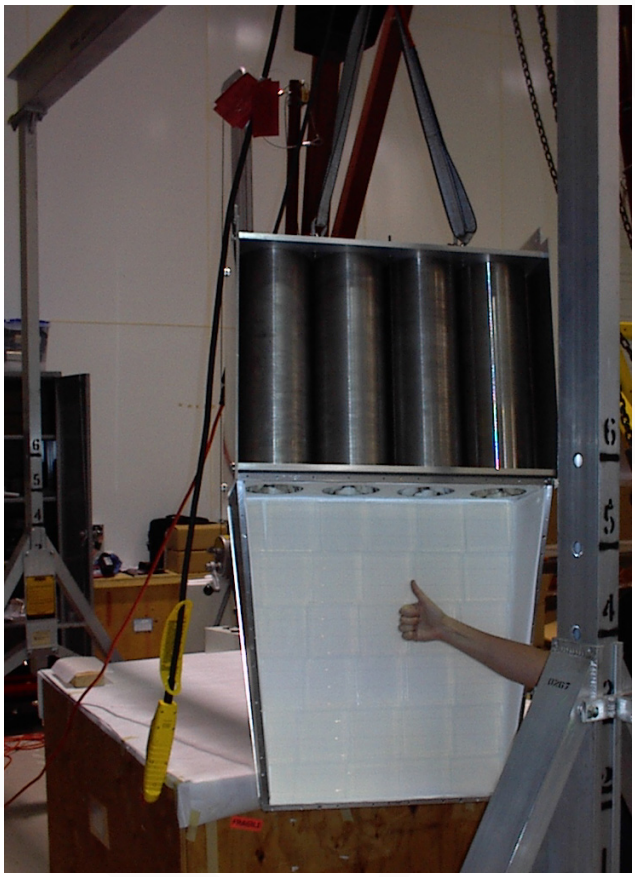

Fig. 2 The production version of the aerogel Čerenkov detector after arrival at Jefferson Lab. The detector box is filled with aerogel tiles and the "tile-retainer" system has been installed.

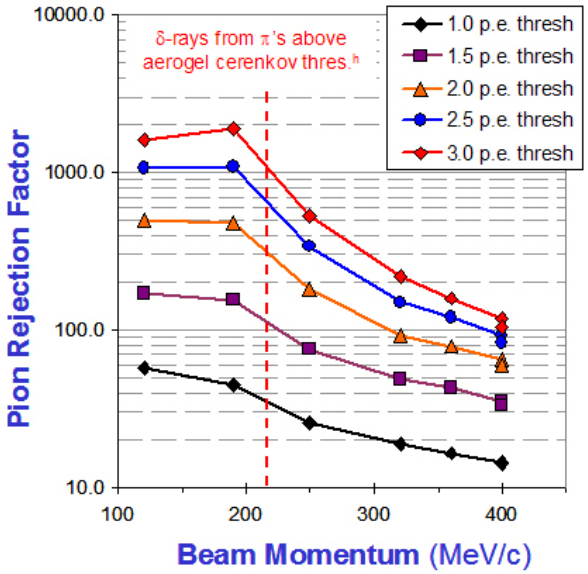

Fig. 4 The Čerenkov detector pion-rejection factors as a function of beam energy, for various threshold settings.

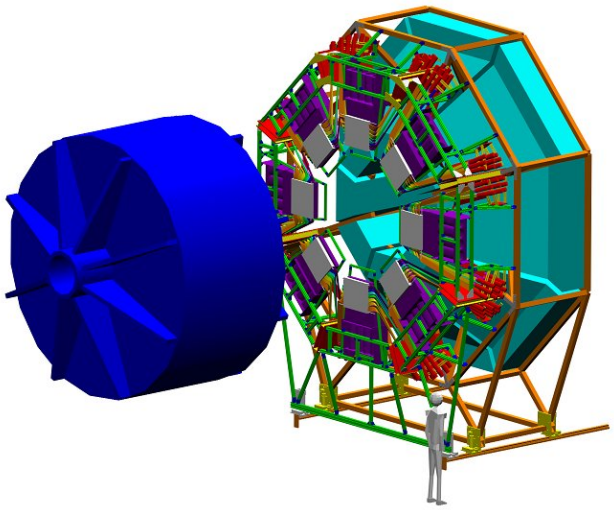

Fig. 5 Conceptual layout of the $G\emptyset$ backward angle configuration.

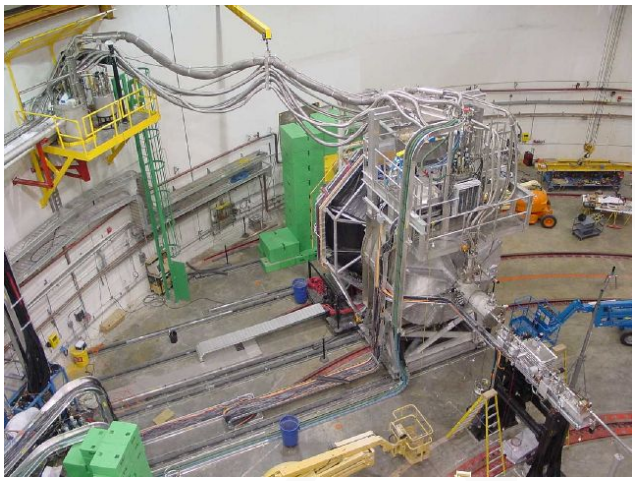

Fig. 6. The $G\emptyset$ apparatus installed in Hall C at Jefferson Lab. The beam enters from the lower right. From right to left, we see the $G\emptyset$ beam monitoring girder, the LH_2 target service module, the 8-sector superconducting magnet, the detector Ferris wheel, and the green shielding wall.

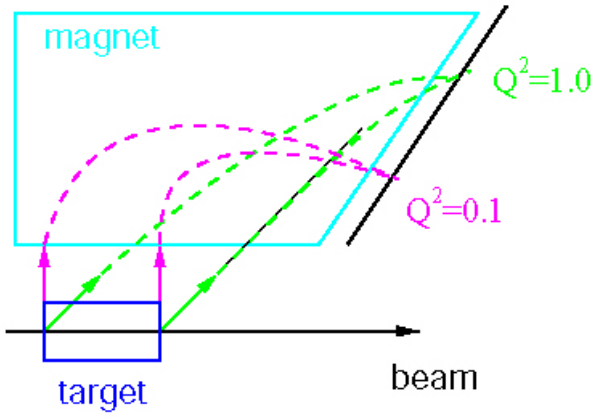

Fig. 7. Principle of the forward angle measurement. Recoil protons corresponding to a given momentum transfer are focused on a specific focal plane detector regardless of where in the target they originate.

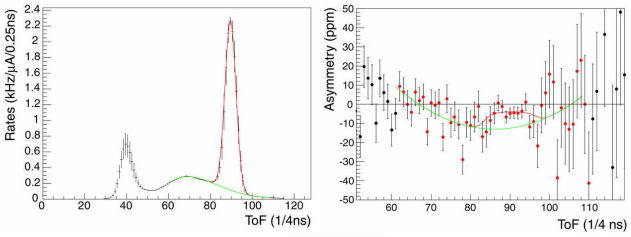

Fig. 8. Fitting of the yield and the asymmetry. In left panel the background under the elastic peak is shown fitted with a fourth order polynomial and the peak itself with a Gaussian. The background asymmetry (right panel) is fitted with a second order polynomial.

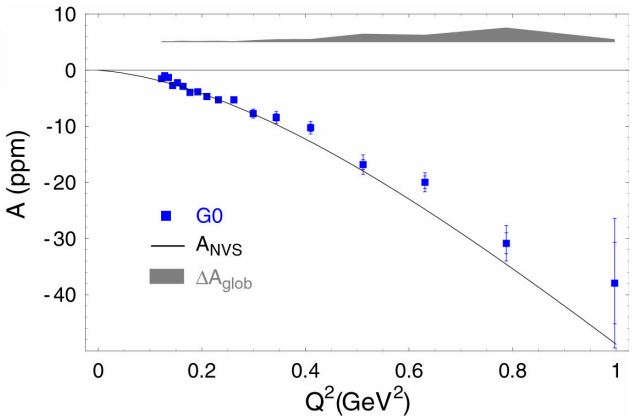

Fig. 9. Experimental analyzing powers measured by $G\emptyset$. The inside error bars are statistical and the outside error bars include point-to-point systematic errors. The grey band shows global systematic errors that affect more than one point. The solid line is the "no vector strange" curve calculated using Kelly's values for G_E and G_M and assuming that G_E^s and G_M^s are zero.

Fig. 10. A single backangle octant, complete with CEDs and Čerenkov detector installed, rotated by 180° into the "Octant-5" orientation.

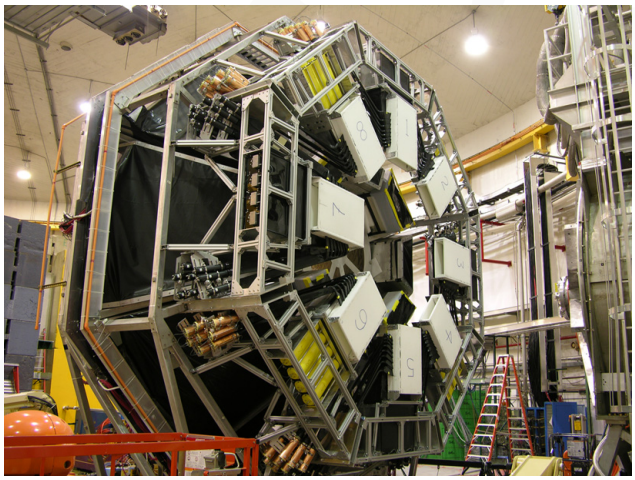

Fig. 11. The fully-assembled mini-Ferris wheel structure supporting the front-end detectors is shown mounted onto the existing Ferris wheel detector support structure in Jefferson Lab's Hall C.

TJNAF Experiment 02-020
The Q_{weak} experiment: a search for physics at the TeV scale via a measurement of the proton's weak charge
(S.A. Page, Manitoba)

Background

Precision measurements of parity violation have traditionally played a key role in guiding our understanding of the electroweak interaction. A key prediction of the Standard Model is the variation of the weak mixing angle, $\sin^2\theta_W$, with momentum transfer Q^2, referred to as the "running of $\sin^2\theta_W$". As with the QED and QCD couplings, $\alpha(\mu^2)$ and $\alpha_s(\mu^2)$, $\sin^2\theta_W(\mu^2)$ is an effective parameter defined at a scale $\mu^2 \sim Q^2$ at which a given experiment is performed. The μ-dependence arises from loop corrections to the electroweak gauge couplings, and thus reflects the content of the Standard Model beyond tree-level. Physics beyond the Standard Model influences the running of $\sin^2\theta_W$ via the incorporation of new diagrams in corrections to the electroweak gauge couplings.

Thus far, measurements at the Z^0 pole have constrained $\sin^2\theta_W$ to impressive precision at that energy scale, and a few experiments have attempted to establish the expected running of $\sin^2\theta_W$ to lower energies, with less certain results. Higher precision experiments to determine $\sin^2\theta_W$ at low energy are needed to complement the Z^0 pole measurements and constrain new physics beyond the Standard Model.

The Standard Model running of $\sin^2\theta_W$ predicts a shift of $+0.007$ at low Q^2 with respect to the Z^0 pole best fit value of 0.23113 ± 0.00015. Figure 1 shows a calculation by Erler and Ramsey-Musolf [Phys. Rev. **D72**, 073003 (2005)] for $\sin^2\theta_W$ together with existing and proposed world data. The expected evolution of $\sin^2\theta_W$ corresponds to a 10 standard deviation effect in the planned Q_{weak} experiment at Jefferson Laboratory, including both experimental and theoretical systematic errors. Any significant deviation from the Standard Model prediction would be a signal of new physics, whereas agreement would place new and significant constraints on possible Standard Model extensions.

High energy studies which determine $\sin^2\theta_W$ at the Z^0 pole are complementary to the precision low energy experiment described here. The precise Z^0 pole measurements set the overall magnitude of the $\sin^2\theta_W$ curve, while additional experiments at low energy are required to establish the running with energy scale. Low energy values of $\sin^2\theta_W$ have been extracted from parity violating Möller scattering [Anthony *et al.*, Phys. Rev. Lett. **95**, 081601 (2005)], atomic parity violation [Bennett and Wieman, Phys. Rev. Lett. **82**, 2484 (1999); Wood *et al.*, Science **275**, 1759 (1997)] and

neutrino deep inelastic scattering experiments [Zeller *et al.*, Phys. Rev. Lett. **88**, 091802 (2002)], but significant uncertainties in the theoretical interpretation of the latter limits the impact of the results. In contrast, the precision measurement of the weak charge of the proton, $Q_w^p = 1 - 4\sin^2\theta_W$, under construction at Jefferson Lab [TJNAF Proposal E02-020 (2004)] with major involvement of the Canadian group and the strong support of TRIUMF infrastructure, addresses similar physics issues but is free of many-body theoretical uncertainties and is designed for significantly better precision.

Experimental overview

The proton's weak charge, $Q_w^p = 1 - 4\sin^2\theta_W$, will be evaluated from a precision measurement of the parity violating asymmetry in elastic electron-proton scattering at very low momentum transfer. The parity-violating asymmetry A is the ratio of the helicity dependent part of the cross section for ep elastic scattering to the helicity average cross section:

$$A = \frac{\sigma_+ - \sigma_-}{\sigma_+ + \sigma_-} \ . \qquad (1)$$

At small scattering angles and low momentum transfer, the asymmetry can be written as:

$$A = \left[\frac{-G_F}{4\pi\alpha\sqrt{2}}\right]\left[\, Q^2 Q_w^p + Q^4 B(Q^2)\right] \ . \qquad (2)$$

Neglecting radiative corrections, the leading term in Eq. 2 is the proton's weak charge: $Q_w^p = 1 - 4\sin^2\theta_W$. The quantity $B(Q^2)$ is the leading term in the nucleon structure defined in terms of neutron and proton electromagnetic and weak form factors. These structure contributions can be reduced by carrying out the asymmetry measurements at lower momentum transfer, but at the expense of reduced sensitivity to Q_w^p. The value of $B(Q^2)$ can be determined experimentally by extrapolation from the ongoing program of forward angle parity-violating experiments at higher Q^2. The optimum value of Q^2 for the $\mathrm{Q_{weak}}$ experiment is near 0.03 $(\mathrm{GeV}/c)^2$. At this momentum transfer, the parity violating asymmetry is expected to be $A = -0.3$ ppm, and we must achieve a total uncertainty of 2% in the measurement of A in order to meet our precision goal of 0.3% in $\sin^2\theta_W$. The contributions of the weak charge and structure dependent terms to the parity-violating asymmetry at 0.03 $(\mathrm{GeV}/c)^2$ are expected to be:

$$\begin{aligned} A &= A_{Q_w^p} + A_{\mathrm{Had}_V} + A_{\mathrm{Had}_A} \\ &= -0.194\,\mathrm{ppm} - 0.077\,\mathrm{ppm} + 0.002\,\mathrm{ppm} \end{aligned} \qquad (3)$$

where the hadronic structure contributions are separated into vector and axial vector components [Young, private communication (2006)].

Table I contains a brief summary of the key uncertainties and error budgets for this experiment. A 2200 hour measurement of the parity violating asymmetry in elastic electron-proton scattering at a momentum transfer of $Q^2 = 0.03$ $(\mathrm{GeV}/c)^2$ employing 180 μA of 85% polarized beam on a 35 cm liquid hydrogen target will determine the proton's weak charge with 4% combined statistical and systematic errors; this in turn implies a determination of $\sin^2\theta_W$ at the $\pm 0.3\%$ level at low energy. The results of previous experiments in parity violating electron-proton scattering will be used to constrain hadronic corrections to the data. A recently published model-independent analysis by Young *et al.* [Phys. Rev. Lett. **97**, 102002 (2006)] of published SAMPLE, PVA4, HAPPEX and $G\emptyset$ data confirms the expected hadronic structure uncertainty listed in Table I for the $\mathrm{Q_{weak}}$ experiment. We note that as a stand-alone measurement of $\sin^2\theta_W$, the $\mathrm{Q_{weak}}$ experiment is competitive with any channel measured in the recently completed SLD and LEP programs at the Z resonance.

The layout of the experiment is given in Fig. 2. A longitudinally polarized electron beam, a liquid hydrogen target, a room temperature 8-fold symmetric toroidal magnetic spectrometer, and a set of detectors for the scattered electrons at forward angles are the key elements of the experimental apparatus. The toroidal magnetic field will focus elastically scattered electrons onto a set of 8, rectangular quartz Čerenkov detectors coupled to photomultiplier tubes, which will be read out in current mode to achieve the high statistical precision required for the measurements. Inelastically scattered electrons are bent out of the detector acceptance by the spectrometer and make only a minimal contribution to the Čerenkov signal.

Basic parameters of the experiment are summarized in Table II. The main technical challenges result from the small expected asymmetry of approximately –0.3 ppm; we will measure this asymmetry to $\pm 1.8\%$ statistical and $\pm 1.4\%$ systematic errors. Fixing $Q^2 = 0.03$ $(\mathrm{GeV}/c)^2$ limits nucleon structure contributions which increase with Q^2 while avoiding very small asymmetries where corrections from helicity correlated beam parameters begin to dominate the measurement uncertainty. With these constraints applied, the figure-of-merit is relatively insensitive to the primary beam energy; using a higher beam energy would result in a physically longer experiment with stronger magnetic field requirements, smaller scattering angles, and the possibility of opening new secondary production channels that might contribute to backgrounds.

The Q_{weak} magnetic spectrometer QTOR

Pancake and coil assessment Two days were spent at MIT-Bates in April to inspect the QTOR coils. The pancake control reports issued by SigmaPhi contained a number of inconsistencies. For example, their reports for the coil width contained left-arm, internal, and right-arm measurements, as well as the total width measurement. These sometimes disagreed by as much as 5 mm. (A similar statement applies to the coil length measurements.) The first objective was thus to reconcile these discrepancies by making additional on-site measurements. Although the epoxy coating on the coils appeared fairly transparent, locating the actual edges of the copper turns was not that easy. (Because of the rounded corners of the conductor a systematic shift in locating the apparent edges could easily be made.) Thus, these on-site measurements also had their uncertainties. In the end a reasonable compromise could be made, with adjustments to about twenty of the SigmaPhi measurements.

The coil control reports issued by SigmaPhi provided measurements of the potted coil sizes as well as detailed information on the alignment of the two pancakes in the coil. With respect to the latter, the reports could not be reconciled with the information on the individual pancakes. Fortunately, inspection of all the coils revealed a fairly consistent picture; the sides and ends of the two pancakes appeared to be aligned as well as one might have anticipated.

From the results discussed above, a good understanding of the location of the copper in the actual coils was established. Uncertainties of a few mm are likely still present in the location of an occasional turn but, averaged over all turns, this uncertainty should be much less and have minimal consequences. Specific information and instructions arising from the above on aligning the coils in assembling QTOR have been forwarded to Karen Dow at MIT.

Compared with the original drawings issued for QTOR, the manufactured coils are, on average, 10 mm wider, 16 mm shorter, and have a straight section which is 22 mm shorter. The pancake widths (except for coil 1, the spare) are well within the revised specifications of 1483 ± 4 mm, while the pancake lengths, with revised specifications of 3679 ± 3 mm (layer 1) and 3639 ± 3 mm (layer 2), are generally in good agreement (Fig. 3).

New magnetic field map All the details of the manufactured coils, the inter-pancake and inter-coil connections and the current-return loop have been incorporated into a revised computer code for calculating the QTOR magnetic field. Because of the coil to coil variations, the field in each sector is slightly different. The new field map reflects this fact by providing the field values for each of the eight sectors. Because of the large number of field points required this new map covers only the envelope of the elastic electrons. The old map is copied to all sectors to cover the regions outside the elastic envelope. It should be noted that the distance of the coil centre line from the beam axis has been set at 36.00 in. in these calculations. This distance is still subject to change (35.75 in. vs. 36.00 in.).

As a first test of this revised magnetic field, a family of trajectories ($\theta = 6°$, $9°$, $12°$ and $\phi = 0°$, $\pm 10°$, $\pm 14°$) was traced through each of the eight sectors. The angles θ and ϕ are specified at the target, a distance of 650 cm from the centre of the magnet. Averaged results for the eight sectors are shown in Fig. 4, where the intersections of the scattered electrons with the detector bars are illustrated. The x and y coordinates are measured transverse and along the bars, respectively, from the centre of the bar. The standard deviations of each of these points, arising from the sector to sector variations, are about $\sigma_x = 0.05$ cm and $\sigma_y = 0.09$ cm, an acceptable spread.

Zero-crossing analysis and field mapping Using field-mapping equipment developed at TRIUMF, two types of measurements will be made to assess the QTOR magnetic field. Absolute field strengths will be determined along the central electron trajectories to verify that the associated $\int Bdl$ is matched to a level of 0.4% for all sectors. In addition to the absolute field measurements, zero-crossing measurements will be made to determine all coil positions to $\approx \pm 1.5$ mm and coil angles to $\approx \pm 0.1°$.

The ability of zero-crossing measurements to determine the coil positions has been tested in realistic simulations, and provided excellent reproduction of the actual coil displacements. The latter were calculated from random distributions of $\sigma_{XYZ} = 0.25$ cm and $\sigma_{\mathrm{ANG}} = 0.1°$. The results are shown in Fig. 5.

The Q_{weak} current mode electronics

Progress summary Since our last report, 10 dual preamplifiers comprising 20 channels have been delivered to Jefferson Lab for use on the main detectors. These units have been set to permit gain selection of $V_{\mathrm{out}}/I_{\mathrm{in}} = 0.5$, 1, 2, or 4 M$\Omega$. Additional preamps for the luminosity monitors and other beam line instrumentation with a gain selection of $V_{\mathrm{out}}/I_{\mathrm{in}} = 0.5$, 1, 25, or 50 M$\Omega$ are now being built at TRIUMF. In all, a total of 28 dual preamps are required, 14 "main detector" style and 14 "lumi" style. In addition, a prototype VME 8-channel digital integrator has been built and delivered to Jefferson Lab to be tested with the Q_{weak} DAQ. In preliminary bench tests at TRIUMF under realistic operating conditions, the module performed

well.

Parity violating signal Each of the 16 photomultiplier tubes of the Q_{weak} main detectors will deliver a signal of about 6 μA to the current mode electronics. As illustrated in Fig. 6, this signal is expected to change by a very small amount when the helicity of the incident electron beam is reversed. Assuming a longitudinal polarization of 85% and a parity-violating longitudinal analyzing power of –0.3 ppm, the 6 μA signal will only change by 3 pA when the spin is flipped. Such a small signal can only be extracted from the noise by using synchronous data acquisition and running for long enough that random noise cancels out.

Data acquisition The experiment plans to use relatively rapid spin flip. Each spin state will last only 4 ms, followed by a short time during which the data are read out and the Jefferson Lab ion source changes state (Fig. 7). The TRIUMF current mode electronics consists of low noise current-to-voltage preamplifiers followed by digital integrators. The integrators are triggered at the start of each spin state and integrate for the precise pre-set spin duration. The system clock of all the digital integrators will be slaved to the same 20 MHz clock used to generate the spin sequence at the ion source. We plan to use the spin sequence $(+--+)$ or $(-++-)$ to cancel linear drifts over each spin quartet.

Digital integrators Figure 8 shows the layout of an 8-channel digital integrator. When triggered, the device integrates all the input signals for a preset time. The integration time and many other parameters can be set through the VME bus. A prototype was tested at TRIUMF using a current source and the same preamplifier to be used on the Q_{weak} experiment. Figure 9 shows the $A_z = (N_+ - N_-)/(N_+ + N_-)$ values calculated assuming $(+--+)$ quartets. Of course, no spin flip was really involved so we expect the values to centre around zero. The rms spread on the 16 ms A_z values was ∼3 ppm, implying that a precision of 2×10^{-9} can be obtained in a 10 hour run. While such low noise is far lower than required during production running (over three orders of magnitude below counting statistics), it will enable us to do important null-asymmetry control measurements in a reasonable time. Tests using only the preamp and input cable show that purely electronic noise only contributes 1.4 ppm to a 16 ms determination of A_z, corresponding to 1×10^{-9} for a 10 hour run.

Systematic errors for Q_{weak}

Now that the QTOR coils have been manufactured, a new magnetic field map has been produced by Peiqing Wang and Willie Falk that is based on the actual dimensions of the coils. The old map was generated for just one sector of QTOR with magnetic field components rotated suitably for use in all eight sectors. As the QTOR coils are not identical, the new map has slightly different fields in each sector, so the map covers all eight sectors. The new map follows the envelope of elastically scattered electrons and is merged with the old map outside that region.

Previous estimates of systematic errors due to beam properties that change on spin flip assumed eight-fold symmetry for QTOR – the rate on one Čerenkov bar was calculated as a function of position of beam on target, for example, and that rate map was used for all eight sectors with suitable rotations of coordinates. The false asymmetries seen by the eight Čerenkov bars were therefore related. Because perfect eightfold symmetry was assumed, some components of the asymmetry cancelled exactly when an average was taken over all bars.

This approach could be extended with the new eight sector field map. This is not feasible in practice, however, as the eight-fold symmetry is broken and so fits to rate would need to be made for each bar separately, and then the fits compared to assess how well asymmetries cancel. An approach using a global fit for all eight bars together should yield results of greater statistical significance. This has been achieved by calculating asymmetries from the summed signal of all eight Čerenkov bars. There is the added advantage that fits to the sum are simpler than fits to individual bars because of the greater symmetry of a complete ring of bars. Asymmetries will be measured in both ways in the actual experiment – the average of eight separate bar asymmetries and the asymmetry from the sum of all eight bars.

The net false asymmetries from the two methods should be the same if the bar signals are matched, as can be seen as follows. Individual detector rates are measured as a function of position (x, y) of beam on target, for example, and are fitted by:

$$R_1(x,y) \sim 1 + a_1 x + b_1 y + c_1 x^2 \ldots , \quad (4)$$

$$\vdots \quad (5)$$

$$R_8(x,y) \sim 1 + a_8 x + b_8 y + c_8 x^2 \ldots . \quad (6)$$

Asymmetries are calculated for all eight bars and averaged, leading to an average false asymmetry of:

$$\epsilon = (\bar{a} + 2\bar{c}x_0 + \ldots)\delta x , \quad (7)$$

where the beam is at $x^{\pm} = x_0 \pm \delta x$ in the two spin states, the average values of the coefficients are taken and the relative sizes of bar signals cancel. When the bar signals are summed, the overall rate is:

$$R(x,y) \sim 8(1 + \bar{a}x + \bar{b}y + \bar{c}x^2 \ldots) , \quad (8)$$

giving the same false asymmetry as before with the proviso that the bar signals must be normalized correctly relative to one other. The effect of mismatching bars will be considered below. In any case, the asymmetry calculated from the sum of perfectly matched bar signals results in the same net asymmetry as when individual bar asymmetries are averaged. Results of simulations with an order of magnitude higher statistics than before are presented below.

Errors due to motion of beam To determine the sensitivity to beam motion, a simulation determined the summed rate on the eight bars as a function of position (x, y) of beam on target for 44 million events hitting the bars. The distribution of this rate was then fitted by:

$$R(x, y) \sim 1 + ar^4 \,, \tag{9}$$

with $r = \sqrt{x^2 + y^2}$, $a = -0.0163 \pm 0.0003$ cm^{-4} and the reduced chi-square is $\chi^2_\nu = 1.18$. In principle, there should be eight-fold symmetry, but it was not visible at this level. Previous fits to rates on individual bars with an order of magnitude fewer events implied that the rate should involve an r^2 term rather than r^4. An r^2 fit here yields $\chi^2_\nu = 2.05$. The flatter variation of the r^4 term near the origin leads to lower sensitivity to position and size modulations.

The false asymmetry when the beam moves on spin flip is

$$\epsilon = 4ax_0r^2\delta x \,. \tag{10}$$

If the beam is on the x axis it should be positioned to within 0.3 cm of $x_0 = 0$ to keep the false asymmetry less than 6×10^{-9}, if $\delta x = 20$ nm.

The effect of mismatching Čerenkov bar gains can be seen by playing back the Geant Ntuple with a gain factor applied to one or more bars. If the bar centred on the $+x$ axis is given a boost in gain of δg, where the nominal gain is $g = 1$, the summed rate becomes:

$$R(x, y) \sim 1 + ar^4 + bx \,, \tag{11}$$

where a is unchanged and $b = (0.015 \pm 0.003)\delta g$ cm^{-1}, $\chi^2_\nu = 1.19$. The false asymmetry is now:

$$\epsilon = (4ax_0r^2 + b)\delta x \,. \tag{12}$$

The effect of the gain mismatch is to pull the "position neutral axis" where the sensitivity to beam position disappears to $x_0 = (-b/4a)^{1/3}$. The neutral axis would be moved by 1 mm when the single bar gain is changed by 0.4%. Taking the response of all eight bars together and treating the gain mismatch of each as a random variable of standard deviation σ_g, a contribution to the false asymmetry of 6×10^{-9} results when $\sigma_g = 0.1$, i.e., when the gains are set to 10%. As will be shown below, a more stringent requirement on gain setting will result from angle modulation of the beam on target.

Errors due to changing size of beam on target The effect of varying beam size can be found by integrating $R(r) \sim 1 + ar^4$ over radius to find the average detector response as a function of beam size. The false asymmetry induced by a circular beam spot of radius changing with helicity as $r^\pm = r_0 \pm \delta r$ is:

$$\epsilon = \frac{4}{3} a r_o^3 \delta r \,. \tag{13}$$

With $r_0 = 2$ mm to approximate a 4 mm by 4 mm raster, δr should be less than 350 nm to produce a false asymmetry that is no more than 6×10^{-9}.

Errors due to changing angle of beam on target Figure 10 shows the variation of summed rate with the angle of beam on target with 37 million electrons hitting the Čerenkov bars. The beam is directed in the $x - z$ plane to the centre of the target at an angle θ to the z axis. The black (lower) curve is for perfect matching of bar gains and is fitted by:

$$R(\theta) \sim 1 + a\theta^2 \,, \tag{14}$$

where $a = 0.060 \pm 0.015$ deg^{-2}, $\chi^2_\nu = 1.07$. If the angle of beam on target changes on spin flip as $\theta^\pm = \theta_0 \pm \delta\theta$, then the false asymmetry is:

$$\epsilon = 2a\theta_0\delta\theta \,.$$

For a false asymmetry that is less than 6×10^{-9}, $\theta_0\delta\theta$ should be less than 5×10^{-8} deg^2. Setting $\theta_0 = 60$ μrad $\equiv 0.0034°$, the limit on $\delta\theta$ becomes 0.3 μrad.

The red (upper) curve in Fig. 10 shows the effect of boosting the gain of the detector centred on the $+x$ axis by 10%. The distribution is now skewed and follows:

$$R(\theta) \sim 1 + a\theta^2 + b\theta \,, \tag{15}$$

with a unchanged and $b = (0.079 \pm 0.015)\delta g$ deg^{-1}, $\chi^2_\nu = 1.09$. Adding in quadrature the effects of gain mismatches for all of the bars, the resulting value of b is $0.15\sigma_g$ deg^{-1} and the false asymmetry from mismatched gains and misaligned beam is:

$$\epsilon = 0.15\sigma_g\delta\theta \,. \tag{16}$$

With $\delta\theta = 0.26$ μrad $\equiv 15 \times 10^{-6}$ degrees as above, gains should be matched to 0.3%.

Summary Table III summarizes the updated beam requirements and compares with previous results. For size modulation, D is the diameter of the beam. The r^4 dependence of rate as a function of position of beam on target results in a flatter distribution near the origin and lowered sensitivity to beam position and size modulations compared to previous estimates. The variation with angle is estimated here over a smaller range of angles around zero than before. It was found that the summed rate increases for the first 0.5° rather than decreasing as previously thought. This is because one bar gains rate rapidly as the beam is directed toward it. At larger angles that gain is offset by loss of rate in the other seven bars, which is what was seen and fitted previously when a larger angle range was considered. The requirement for matching bar gains is needed only when asymmetries are measured by adding signals from the eight Čerenkov bars.

Q_{weak} focal plane scanner

The quartz scanner detector project was funded by an NSERC Research Tools and Instruments (RTI) award in 2006, and it will benefit from the CFI award to J. Martin at the Univ. of Winnipeg to equip a detector set-up and testing facility. Progress to date includes simulation work to model the reported performance of the E158 scanners, initial prototyping with small detector elements and cosmic ray tests at the Univ. of Winnipeg, and design work on the 2D motion controller in collaboration with Jefferson Lab and the Univ. of Manitoba shops.

The focal plane scanner is a quartz detector which can be operated in counting mode at full beam current and scanned over the focal plane. In addition to running the experiment in tracking mode at very low beam current, it will be important to confirm the electron distribution on the main detectors at the high beam current used for production running without tracking.

We plan to use the scanner to

- map out the acceptance of the main detectors for the experiment, which are quartz Čerenkov bars, in order to benchmark physics and optics simulations. The scanner is necessary to extrapolate spectrometer optics parameters determined at 10 nA using tracking chambers to 180 μA
- determine the behaviour of the main detectors at high beam current by operating the small detector, which will have similar properties, in pulse-counting mode
- to scan into the inelastic region, giving greater confidence in any corrections made for inelastic contributions to the asymmetry
- and to assist in Q^2 determination for the experiment.

The concept and geometry of the scanner is modelled after the similar detector for the SLAC E158 parity-violating Möller scattering experiment. The Q_{weak} scanner would consist of a small quartz radiator of approximately 1 cm^2, residing in an air core light guide, where the light is collected by phototubes. Quartz has been chosen for the main detector because it is radiation hard and does not scintillate, making it relatively insensitive to backgrounds of gammas and neutrons. The scanning detector should also be quartz to match the response.

The detector will be scanned by an xy table using two linear motion modules (see Fig. 11) with associated drive controllers computer interface and software.

Compton polarimeter

To achieve the desired overall accuracy in Q_{weak}, the electron beam polarization must be measured with an absolute uncertainty at the 1% level. At present, this can be achieved in Hall C using an existing Möller polarimeter, which operates at beam currents below 8 μA – the current limit is due to heating and subsequent magnetization loss of the Fe target foils. An R&D program to push the operating range of the Möller polarimeter to higher beam currents has been under way for the past few years; a scheme involving a very thin target that is normally out of the beam and a fast kicker magnet to steer the beam onto the foil for brief periods has demonstrated good performance at average beam currents up to 40 μA.

A major effort to design and build a Compton polarimeter in Hall C at Jefferson Lab is also under way as part of the laboratory's support of this and other experiments where precise beam polarimetry is an issue; the Compton polarimeter will provide a continuous on-line measurement of the beam polarization at full current (180 μA).

The plan for the Compton polarimeter calls for detection of both photons and electrons. To detect the electrons, the Canadian group plans to supply radiation hard diamond strip detectors together with associated readout electronics. The electron detectors will have 2.1 cm × 2.1 cm active area, etched into 100 strips per plane, with segmentation in the bend plane of the magnet chicane for sensitivity to the scattered electron energy. The detector will be housed inside a vacuum pipe and equipped with a linear motion mechanism to retract the detector when not in use and to precisely position it when polarization measurements are being made. Diamond is a semiconductor at room temperature and its properties can therefore be compared with silicon. However, diamond has a band gap of 5.5 eV (compared to 1.12 eV in silicon) resulting in lower leakage currents. Additionally diamond has higher electron

and hole mobilities than silicon, resulting in faster timing properties, and a lower dielectric constant resulting in lower detector capacitance.

The Canadian group has submitted an RTI proposal to NSERC to build a major fraction of the recoil electron detectors and associated readout electronics. The proposal will be supported by the detector set-up lab at the Univ. of Winnipeg funded by CFI, technical facilities in the Electrical Engineering department at the Univ. of Manitoba, and we may request TRIUMF infrastructure support for electronics development and testing.

Detector development

A large body of simulation work has been completed, to help in the detector design. All PMTs and magnetic shields have been delivered to Jefferson Lab. The delivery of quartz for the main detectors is nearly complete. The light guides are on order and the detector housing and mounting structures are being designed. Due to very high student participation, there's been good progress recently on quartz bar quality assurance (QA) testing (Fig. 12) and detector design. We have identified several glue candidates and are now ready to perform glue transparency measurements, including radiation damage tests and accelerated aging tests. Scintillation and luminescence tests are currently under way. A number of tests on PMT gain uniformity and linearity have recently been completed and we are nearing the completion of PMT base design. We are on track to finish all detector modules by the end of summer, 2007.

Simulations In 2005 and 2006, extensive simulations were done to help in the design of the Čerenkov detectors. These included simulations performed to determine the optimal Čerenkov detector thickness which simultaneously minimizes contributions to the Q_{weak} error from photoelectron and electron shower noise, simulations to determine the optimal light guide shape and length, PMT mounting scheme, as well as mirroring and wrapping of surfaces to maximize the light yield.

For the most part, the statistical error on the measured Q_{weak} asymmetry is simply given by counting statistics $1/\sqrt{N}$, for a given number (N) of primary electron events in a detector within a certain period of time. In a current mode experiment a deviation from zero RMS width and counting statistics is caused by a variation in the number of photoelectrons (PE) (n_{pe}) for a given event. In this type of experiment, events which produce more or less light than the intended "standard" event can't be discriminated against. So the variation in the corresponding number of PEs (i.e. the variation in the current) contributes to the overall RMS width and therefore produces a deviation from counting statistics. In other words, this deviation sets the resolution on the statistical error. The details of the simulation and results are provided in a separate technical note [Gericke, Main Detectors Light Guide Simulations, Q_{weak} Technical Note 30/06/2006].

The geometry of the light guides and PMT attachment for the main Čerenkov detectors is selected according to light transmission and collection performance as well as spatial constraints set by the distance between neighbouring detectors and freedom for position adjustability in the radial direction. The simulation has been performed using Geant4 and the set-up has been described in a technical note [Gericke, Excess Noise as a Function of Detector Thickness, Q_{weak} Technical Note 07/10/2005]. The PMT position is constrained by the detector assembly geometry to be on the face of the light guide, rather than on the edge. Simulations were performed to verify that the detectors produce enough light yield with this geometry, using various combinations of surface mirroring and wrapping of the Čerenkov bar. A plot of the event rate in the quartz bar and light guides as a function of momentum transfer and electron hit location in the beam left-right direction indicated that the elastic rate on the guides was significantly smaller than on the quartz bar.

PMT tests We received 28, 5 in. PMTs with S20 photocathodes. All 28 PMTs underwent an initial performance test to see if any of them has low quantum efficiency or other obvious hardware problems. In addition, all PMTs were tested for relative quantum efficiency (QE), and linearity tests without base and with various low gain bases were preformed. The PMT gain was measured as a function of the bias voltage to understand the behaviour of the dark current. An initial set of noise measurements was also performed for the PMT and base configuration. Figure 13 shows the comparison between the measured shot noise from dark current in the PMT, the measured electronic noise, and the expected counting statistics shot noise, based on the simulated number of photo electrons for a typical electron event.

The $1/f$ noise component inherent in any noise measurement has been removed using

$$\sigma^2 = \int_0^B 2qI_a \left(1 + \frac{f_c}{f}\right)\, df \ . \qquad (17)$$

At this point, two types of PMT voltage dividers have been built and underwent the tests described above. A third and final divider type is currently being assembled. This is anticipated to be the final low gain divider for the Q_{weak} main detectors, optimizing the overall performance of the detectors.

Students University of Manitoba student, Mitchell Andersen, built and tested several generations of prototype PMT bases this summer. He worked with UV LEDs and Zener diodes and accurately measured PMT gains with a current mode technique. He also contributed greatly to a measurement of PMT nonlinearity to an accuracy of better than 10^{-4}.

University of North Dakota student, Elliott Johnson, designed a prototype support rail which was built in the Jefferson Lab machine shop. He also helped order a custom composite panel to support the glued quartz bars, worked with Jefferson Lab and College of William and Mary Q_{weak} collaborators on quartz bar QA and started a preliminary CAD design of the detector mounting scheme.

Conclusion and outlook

The Q_{weak} experiment is a major new initiative being prepared at Jefferson Lab to measure the proton's weak charge and hence test the Standard Model prediction of the running of $\sin^2\theta_W$ to high precision. Construction of the apparatus is currently under way, with plans to mount the experiment in Hall C during 2009. Extensive simulations of the experiment coupled with a vigorous R&D program and analysis of hadronic form factor contributions that are determined from previous experiments, confirm that our goal of a 4% measurement of the proton's weak charge at low momentum transfer, yielding a 0.3% measurement of $\sin^2\theta_W$, should be well within reach.

Collaborators: M.J. Ramsey-Musolf (Caltech); D. Armstrong, T. Averett, C. Capuano, J.M. Finn, K.H. Grimm (College of William and Mary); K. Myers, A. Opper (George Washington Univ.); C. Keppel (Hampton); T. Forest (Idaho State); P. Bosted, J. Benesch, A. Bruell, R.D. Carlini, S. Chattopadhyay, R. Ent, D.J. Gaskell, J. Grames, A. Lung, D. Mack, S. Majewski, D. Meekins, M. Poelker, G.R. Smith, R. Suleiman, S. Wood, R. Young, C. Zorn (Jefferson Lab); K. Johnston, N. Simicevic, S. Wells (Louisiana Technical Univ.); J.A. Dunne, D. Dutta (Mississippi State); K. Dow, W. Franklin, M. Khol, S. Kowalski, Y. Prok, E. Tsentalovich (MIT); Y. Liang, J. Roche, P. King (Ohio); C.A. Davis (TRIUMF); J. Erler (Univ. Nacional Autonoma de Mexico); R. Jones, K. Joo (Connecticut); J. Birchall, W.R. Falk, M. Gericke, L. Lee, J. Pan, S.A. Page, W.D. Ramsay, W.T.H. van Oers, P. Wang (Manitoba); S. Covrig, F.W. Hersman, M. Holtrop, H. Zhu (New Hampshire); E. Korkmaz, T. Porcelli (Northern BC); G. Cates, K. Paschke (Virginia); J. Martin (Winnipeg); J. Mammei, R. Mammei, N. Morgan, M. Pitt (Virginia Polytechnic Inst.); H. Mkrtchyen (Yerevan Physics Inst.).

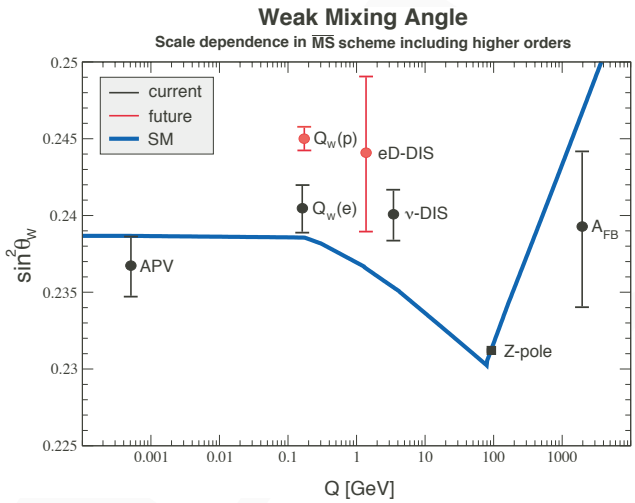

Fig. 1. Calculated running of the weak mixing angle in the Standard Model, as defined in the modified minimal subtraction scheme [Erler and Ramsey-Musolf, *op. cit.*]. The black error bars show the current situation, while the red error bars refer to the proposed 4% Q_w^p measurement and other possible future measurements.

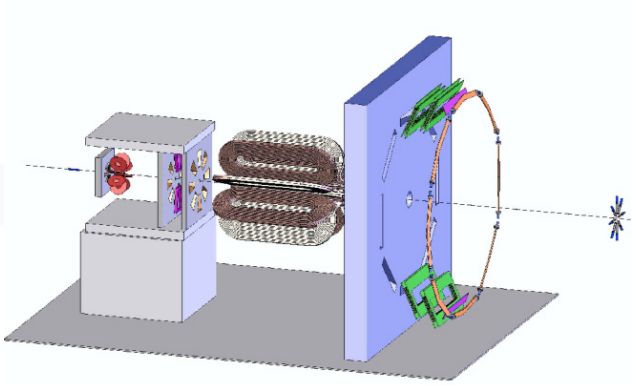

Fig. 2. Layout of the Q_{weak} apparatus. The beam and scattered electrons travel through the target, the first collimator, the region 1 GEM detectors, the mini-torus, the two-stage second precision collimator which surrounds the region 2 drift chambers, the toroidal magnet, the shielding wall, the region 3 drift chambers, the trigger scintillators and finally through the quartz Čerenkov detectors. The tracking system chambers and trigger scintillators will be retracted during high current running when Q_{weak} asymmetry data are acquired. The Q_{weak} luminosity monitor, which will be used to monitor target fluctuations and to provide a sensitive null asymmetry test, is located downstream of the apparatus very close to the beam pipe.

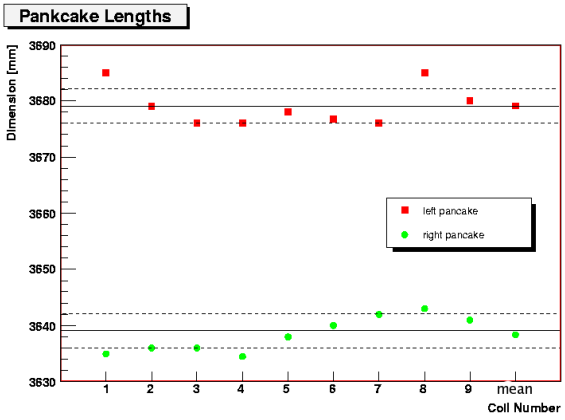

Fig. 3. Pancake lengths for layer 1 (left side) and layer 2 (right side). The distributions, 3679 ± 3 mm for layer 1 and 3639 ± 3 mm for layer 2, are acceptable.

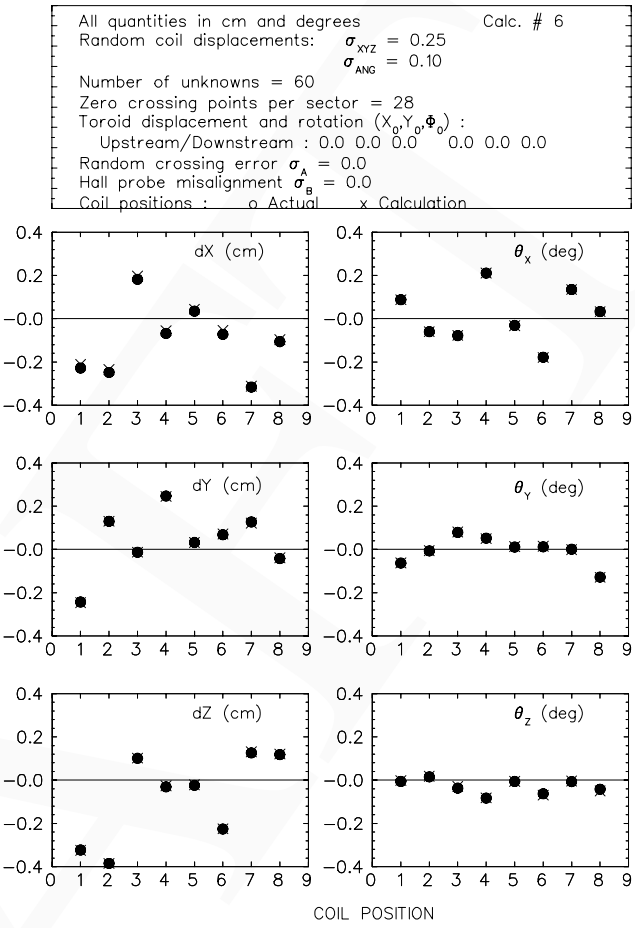

Fig. 5. Simulated coil displacements (solid circles) and the calculated coil positions (crosses) from zero-crossing data expected from the TRIUMF field mapper.

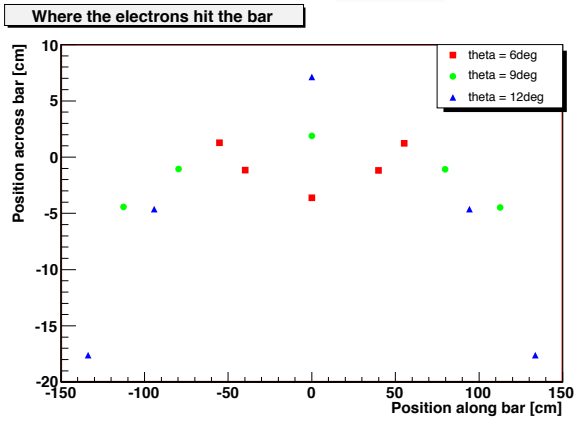

Fig. 4. Averaged trajectory positions for the eight sectors on the detector bars.

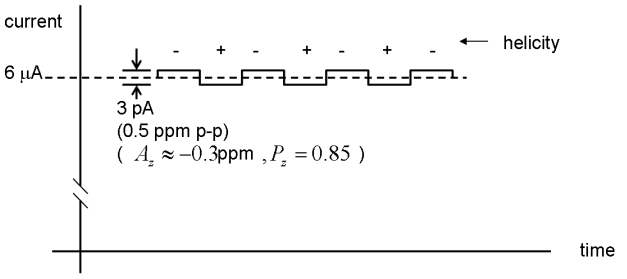

Fig. 6. Small size of the parity violating signal. The 6 μA signal from a main detector is expected to be ∼3 pA greater in the negative helicity state than the positive helicity state. Note the suppressed origin. At the scale of this TRIUMF report, the origin is 3 km off the bottom of the page.

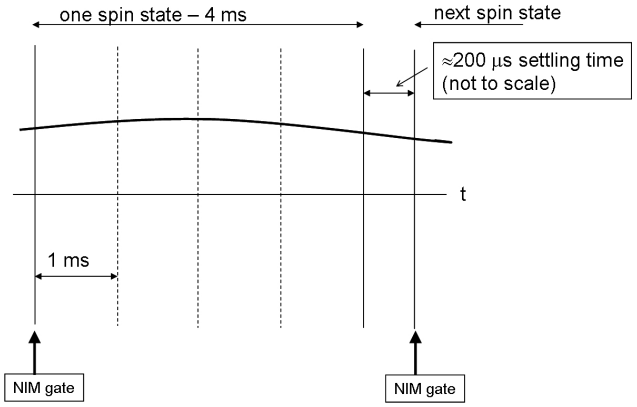

Fig. 7. Data acquisition scheme. Each spin state lasts 4 ms, followed by approximately 200 μs during which the ion source changes state and the electronics is read out. The TRIUMF digital integrator integrates the detector signals over the spin state and stores the result as four 1 ms parts.

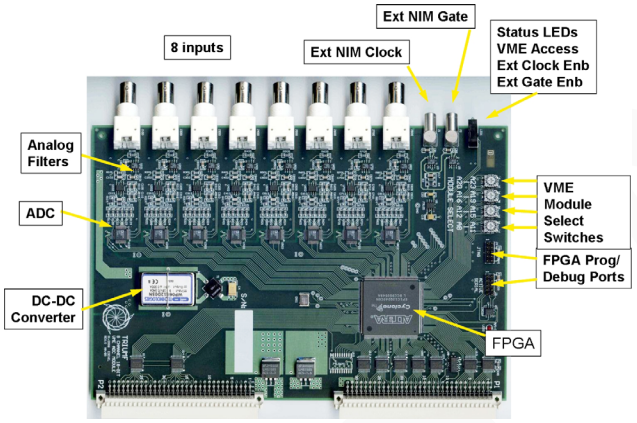

Fig. 8. Layout of the TRIUMF digital integrator. The analogue signals from the 8 inputs first pass through sharp cut-off 50 kHz anti-aliasing filters then are digitized by 18-bit ADCs operating at up to 500 ksps. The field programmable gate array (FPGA) calculates the sums over the selected interval and delivers the results to the VME bus.

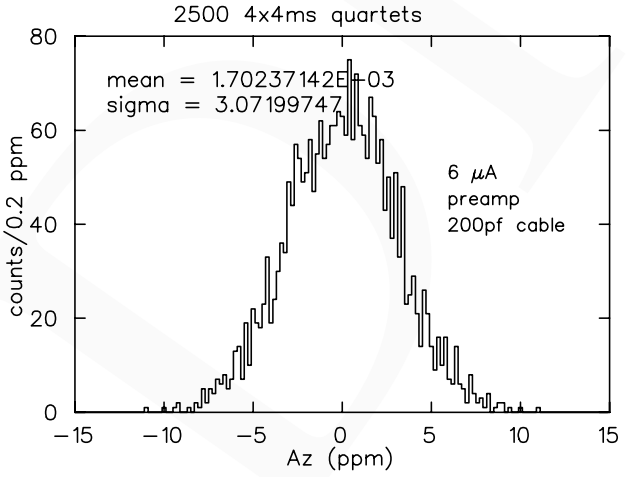

Fig. 9. Realistic test of the TRIUMF digital integrator and preamp. A 6 μA current source feeds the low noise preamp through a cable with a capacitance similar to that expected on the Q_{weak} experiment. The measured A_z values for 16 ms runs (quartets of 4 ms states) have a standard deviation of $\sim$3 ppm, indicating that a statistical precision of 2×10^{-9} can be obtained with a 10 hour run.

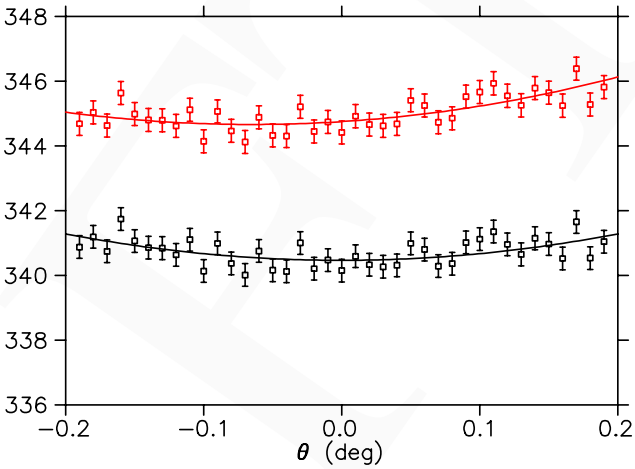

Fig. 10. Event rate summed over all eight Čerenkov bars as a function of the angle of beam on target. For the red (upper) curve, the signal from the Čerenkov bar centred on the $+x$ axis has been increased by 10%.

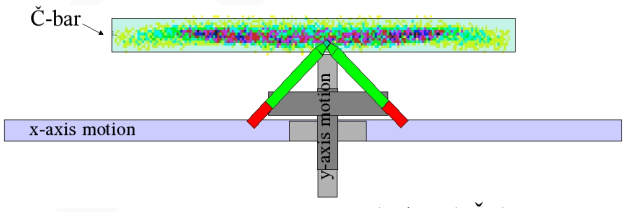

Fig. 11. The scanner is small enough that it can operate in counting mode ($\sim$1 MHz) at full beam current. The $x-y$ scanning mechanism is designed for a full scan of the elastic and inelastic regions.

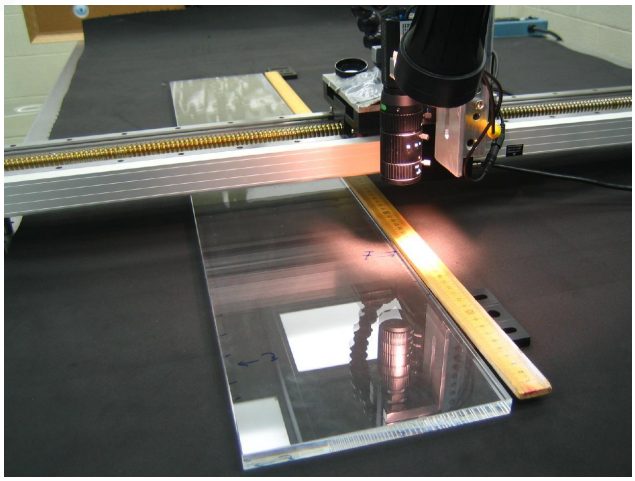

Fig. 12. Set-up for main detector quartz bevel uniformity test.

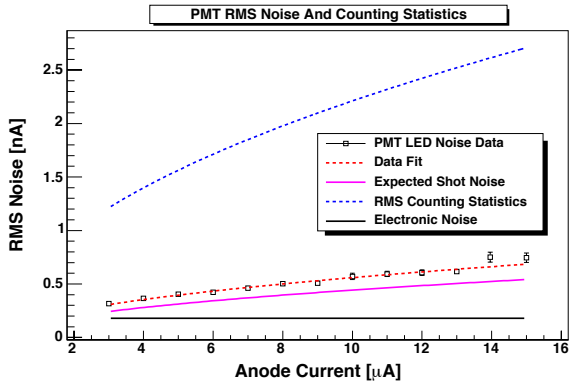

Fig. 13. Comparison of dark current shot noise, electronic noise and electron event shot noise (counting statistics).

Table I. Total error estimate for the Q_{weak} experiment. The contributions to both the physics asymmetry and the extracted Q_w^p are given.

Source of error	Contribution to $\Delta A_{\rm phys}/A_{\rm phys}$	Contribution to $\Delta Q_w^p/Q_w^p$
Counting statistics	1.8%	2.9%
Hadronic structure	—	2.2%
Beam polarimetry	1.0%	1.6%
Absolute Q^2	0.7%	1.1%
Backgrounds	0.5%	0.8%
Helicity-correlated beam properties	0.5%	0.8%
Total:	2.3%	4.3%

Table II. Basic parameters of the Q_{weak}^p experiment.

Parameter	Value
Incident beam energy	1.165 GeV
Beam polarization	85%
Beam current	180 μA
Target thickness	35 cm ($0.04X_0$)
Running time	2200 hours
Nominal scattering angle	8.4°
Scattering angle acceptance	±3°
ϕ acceptance	53% of 2π
Solid angle	$\Delta\Omega = 45$ msr
Average Q^2	0.030 $(\mathrm{GeV}/c)^2$
Average physics asymmetry	–0.288 ppm
Average experimental asymmetry	–0.24 ppm
Integrated cross section	3.9 μb
Integrated rate (all sectors)	6.4 GHz
Statistical error on the asymmetry	1.8%
Statistical error on Q_W^p	2.9%

Table III. Constraints on helicity correlated beam parameters.

Source of error	Error goes as	Condition	Requirement Previous	Present
Position modulation	$x_0\delta x$	$\delta x = 20$ nm	$x_0 < 0.7$ mm	—
	$x_0 r^2 \delta x$	$\delta x = 20$ nm	—	$x_0 < 3$ mm
Size modulation	$D_0\delta D$	$D_0 = 4$ mm	$\delta D < 0.02$ μm	—
	$D_0^3\delta D$	$D_0 = 4$ mm	—-	$\delta D < 0.7$ μm
Direction modulation	$\theta_0\delta\theta$	$\theta_0 = 60$ μrad	$\delta\theta < 1.4$ μrad	$\delta\theta < 0.3$ μrad
Bar gains	$\sigma_g\delta\theta$	$\delta\theta = 0.3$ μrad	—-	$\sigma_g = 0.3\%$
	$\sigma_g\delta x$	$\delta x = 20$ nm	—	$\sigma_g = 10\%$

T2K long baseline neutrino experiment at J-PARC

(A. Konaka, TRIUMF)

Construction of the J-PARC accelerator and T2K neutrino beam line is under way and on schedule. The first stage of the linac was commissioned in the fall and commissioning of the booster is expected in 2007. The first superconducting combined function magnet was constructed and met the specifications. A full-scale prototype horn was constructed and successfully operated at the full current of 320 kA. Very rapid civil construction is in progress, including a large fraction of the beam line tunnel and decay pipe. The commissioning of the beam to fast extraction is scheduled to being on April 1, 2009.

TRIUMF is actively involved in the remote handling design of the target station where the 1 MW beam hits the target. Engineering design of the remote handling mechanism of the final focusing monitor is now done and ready for construction at TRIUMF. Basic design of the service cell with a manipulator system, which will be used for maintenance of the target, horn and beam monitors, is also being done by TRIUMF remote handling engineers (Fig. 1). These beam line

contributions by TRIUMF are supported by the TRIUMF Five-Year Plan.

In April, a 3-year NSERC grant request was approved for the T2K near detector construction. The Canadian T2K detector projects consist of the time projection chambers (TPC), the fine grained detectors (FGD), and the optical transition radiation detector (OTR). The tracker, consisting of three TPCs and the two FGD modules, lies at the heart of the ND280 (see Fig. 2). Its primary function is to measure the neutrino beams flux, energy spectrum, and flavour composition by observing charged current neutrino interactions.

The T2K collaboration continues to grow, including the recent addition of a German group. Currently there are over 300 collaborators from 12 countries. An international collaboration agreement for T2K was formally adopted at the collaboration meeting in November. T2K Canada is a collaboration between the University of British Columbia, University of Victoria, University of Alberta, University of Regina, University of Toronto, York University and TRIUMF.

Time projection chamber progress and status

A large prototype of the T2K TPC field cage has been built and tested. It was read out using large gas electron multiplier (GEM) modules. The resolution performance, as determined with cosmic ray tracks, was found to be in agreement with expectations. There was also work under way in Europe to study micromegas readout modules, using an existing field cage. The T2K spokesperson set up an internal panel to consider the collaboration and resource aspects of the technology choice. This panel finally announced in June that they felt that the T2K collaboration issues argued in favour of using micromegas readout technology. In order to bring the project back on track, all the T2K TPC groups immediately accepted this decision. The T2K TPC group is now working at an accelerated pace in a spirit of strong collaboration. Canada-Europe TPC video meetings are held every 2 weeks.

Organization of the TPC project The TPC project is divided into 9 work packages. The TPC mechanical work package, dealing with all mechanical aspects apart from the micromegas modules, is led by Chris Hearty (IPP/UBC). The TPC gas system work package is being coordinated by Issei Kato, a postdoc at TRIUMF. The integration of the TPC (and FGD) into the experimental hall in Japan is part of the work package led by Roy Langstaff at Victoria. Oversight and coordination of the entire TPC project is the responsibility of Dean Karlen (Victoria) and Marco Zito (Saclay).

Completion of the TPC mechanical design Finalizing the many parameters in the TPC design began at the collaboration meeting in July. Detailed conceptual drawings have been completed for most of the TPC (Fig. 3). The drawings are being converted into 3D format, from which the machining drawings will be derived.

The large router that will be used for the precision machining of the wall panels and endplates is now being commissioned at TRIUMF. Materials for construction of the pre-production module have been ordered. Electron drift studies with the materials are under way in a test cell, in order to verify low electron attachment. Structural tests of the wall panel joints have verified they have the necessary strength.

Finalizing the TPC gas system design The technology choice has had an impact on the gas system, since a mixture with isobutane is now preferred. To keep costs under control, a mixing system will be used, rather than using pre-mixed gases. The gas system design has progressed significantly, and has benefited from consultation with gas experts at CERN and elsewhere. The design will maintain a small pressure difference (0.1 mbar) between the inner and outer gas volumes.

Status of micromegas modules Full size micromegas modules (34 cm $\times$ 36 cm) with the final pad geometry (6.9 mm $\times$ 9.7 mm) have been built at CERN for initial tests. A cleaning procedure has been developed with the goal of limiting the current between the mesh and all pads to less than a few nA at operating voltages.

Status of TPC electronics The TPC readout electronics, the responsibility of the Saclay group, is based on a new ASIC design. The first tests of the initial ASIC production run have been successful. There is no indication that a second iteration in the design is needed. The same ASIC will be used for readout of the FGD modules.

Milestones A full size preproduction TPC module (module-0), will begin construction in 2007. It is intended to undergo tests with prototype micromegas modules and readout electronics at TRIUMF. The construction of the three production modules will commence shortly thereafter, to be ready for testing and shipping to Japan for installation in summer, 2009.

Fine grained detector progress and status

Organization The FGD group has arranged itself into twelve well-defined work packages organized around components such as scintillator, fibres, front-end electronics, photosensors, etc. A subconvener has been assigned for each work package, and no responsibilities are unassigned. The University of Regina group has taken responsibility for the wavelength-shifting fibre work package, which includes procurement, mirroring, polishing, and testing. The University of Vic-

toria group has taken on responsibility for portions of the FGD electronics. Kyoto University has also joined the FGD group, and is taking responsibility for providing and testing the FGD photosensors and optical couplers. The Kyoto group has received funding from MEXT in Japan for these items. Collaboration between the Canadian and Japanese FGD groups is coordinated through an MOU signed by the two groups. A full GANTT chart with assigned resources exists for the FGD project.

Photosensors The FGD will use pixellated avalanche photodiodes operated in Geiger mode to read out the scintillator bars. In 2006 the T2K group tested preproduction photosensors from Hamamatsu Photonics in Japan and from CPTA in Russia. These photosensors have been characterized in terms of photon detection efficiency, gain, noise, pulse shape, and crosstalk. These tests include beams tests in which individual FGD channels have been instrumented and tested in a muon beam. Devices from both manufacturers satisfy the FGD's requirements, and have been shown to have acceptably small failure rates ($\sim$1%) after long-term operation. Hamamatsu has listed their devices in their January, 2007 catalogue and will soon begin mass production.

Mechanical design A complete mechanical design for the FGD has been reviewed internally by the group and submitted to the TRIUMF Design Office. Production of dimensioned design drawings and engineering reviews is nearly complete. The final design hangs XY scintillator modules inside a light-tight box, with electronics mounted in mini-crates around the four sides of the box. This design separates the photosensors and scintillator from heat-producing electronics, which are cooled by negative-pressure water cooling lines around the periphery of the box, and allows easy access to the front-end electronics.

Scintillator production Following R&D runs in February and May, the FGD group, in collaboration with Celco Plastics in Surrey, BC, succeeded in producing high quality square scintillator bars from doped polystyrene including a TiO_2 reflective outer coating and a central hole. Beams tests in the summer established that these bars give sufficiently high light yield for minimum ionizing particles, and in November the group carried out its final scintillator production run. In 16 days of continuous production over 11,500 usable bars were produced. Each bar was labelled with a bar code, checked for blocked holes, and had its width measured immediately after production. The mean bar width was 9.62 mm, with an RMS spread of 0.02 mm, while the TiO_2 coating thickness of 0.25 mm was controlled to $<$0.05 mm (Fig. 4).

Several hundred bars from across the production run have been tested in an automated bar scanner using a radioactive source, and yield an RMS variation in the total light yield of 4%, with no non-Gaussian tails evident.

Gluing of scintillator bars to produce XY modules will begin in January, 2007. Tests of a number of adhesives have selected an epoxy that gives strong bonds and mechanical strength. A half-height XY module was constructed as a test to verify the module design.

Electronics The FGD group has converged on a design based on waveform digitization of the photosensor signals. The proposed design uses the same custom ASIC with a switched capacitor array that will be used for the T2K TPC readout. Photosensor signals are stretched by a preamp/shaper with a 100 ns peaking time, then digitized at 50 MHz. Each mini-crate of electronics contains several front-end boards, one control board that commands and reads out the front-end boards, and a light pulser board. Data are collected by data collector cards outside the magnet over optical links. This year the FGD group has tested a mockup of the digitization path, a prototype board based on the new ASIC, and slow control prototypes. The chosen design is very similar to the TPC electronics architecture, and shares some hardware in common (e.g. the ASIC, the data collection cards). This will result in synergy with the TPC effort and the likelihood that some FPGA programming and data handling software could be recycled.

Simulation The FGD group carried out several simulation studies in 2006. Simulations of individual scintillator bars were used to determine the optimal bar geometry and minimum requirements for light yield based upon the hit efficiency. Another simulation study has developed a new means of separating charged-current quasi-elastic (CCQE) events from non-CCQE events based upon tagging Michel electrons produced in the FGD from stopping pions. This technique increases the CCQE purity well above that obtained by K2K's similar Scibar detector, and provided design constraints for the electronics. Finally, hit-level simulation studies of the entire tracker (FGDs and TPCs) have been done to estimate the event efficiencies and purities.

The optical transition radiation monitor

The purpose of the T2K optical transition radiation (OTR) monitor is to measure the position and width of the proton beam at J-PARC just upstream of the graphite target for T2K. The position and direction of the primary proton beam need to be measured at the target with a precision of 1 mm and 0.5 mrad, respectively, in order to properly estimate off-axis alignment

effects. Monitoring the beam width to an accuracy of 1 mm is necessary to protect the target. The expected position resolution of the beam of the current design of the OTR system is better than 0.5 mm and the expected width resolution is better than 0.5 mm.

The OTR system utilizes the optical transition radiation produced when the proton beam travels through a thin foil. Due to the high-radiation environment the monitor components have to be at some distance away from the foil. A series of mirrors will focus and transport the visible light several metres through channels in the concrete and iron shielding to a camera, as shown in Fig. 5. The resulting image provides information about the shape, size and orientation of the proton beam.

Over the past year, progress has been made in key areas of the system design, and these are highlighted below.

Prototype A 15% scale model of the optical system was tested in June at an electron beam at NRC of an equivalent γ to the J-PARC proton beam. The light was detected down to a beam current of 10 nA, which is the equivalent of 0.5% of a 750 kW beam of 40 GeV protons. The measurements made with the OTR prototype were within 10% of the expected beam size and within 0.5 mm of the expected beam position.

Optical design The system will be composed of 4 parabolic 90° off-axis mirrors. We have identified several potential manufacturers, and have obtained quotations for these mirrors. Suppliers have also been located for the radiation-hard camera and the micro-channel plate that will act as an image intensifier and fast shutter. Our ray-tracing simulations of the optical system indicate that the image resolution is adequate. We have also verified this with commercial ray tracing software.

Mechanical design Significant progress has been made on the mechanical design. The foils will be supported in a rotating disk to allow for periodic foil replacement. The foil holder will then be attached to an arm on the target plate. The mirrors will sit inside vertical tubes that are attached to the front plate. The tubes will keep the mirrors aligned, and will provide some protection from dust. The entire mirror and tube system is designed so that the tubes can be easily removed from above, with a crane, if it is necessary to replace a mirror.

Material selection The choice of mirror and foil materials is crucial due to the large amount of radiation that they will be exposed to. We irradiated several candidate foils and mirrors at the 500 MeV proton beam at TRIUMF in December, and we plan further tests in 2007. A remote camera was used to examine the exposed samples and no significant colour changes were observed.

Calibration There is a certain amount of distortion inherent in the optical system, especially for points on the foil that are far away from the central optical axis. This can be corrected by applying a polynomial warping that translates points in the undistorted image to points in the distorted image. The polynomial coefficients can be determined by using calibration points at known locations. We are investigating placing small holes (that can be backlit) in the foil edges, or using front lighting to illuminate a grid pattern etched in the foil by a laser.

Collaborators: P. Kitching (Alberta); M. Bryant, K. Fransham, C. Hearty, B. Kirby, T. Lindner, D. Maas, S. Oser, D. Roberge, J. Wendland (UBC); M. Barbi, E. Mathie (Regina); R. Tacik (Regina/TRIUMF); M. Cadabeschi, A. Marino, J. Martin (Toronto); P. Amaudruz, D. Bishop, H. Coombes, J. Doornbos, W. Faszer, M. Gallop, P. Gumplinger, R. Helmer, R. Henderson, I. Kato, N. Khan, A. Konaka, L. Kuchaninov, C. Mark, A. Miller, D. Morris, K. Olchanski, R. Openshaw, J.-M. Poutissou, R. Poutissou, F. Retiere, P. Vincent, K. Wong, S. Yen, (TRIUMF); D. Karlen (Victoria/TRIUMF); N. Braam, C. Hansen, R. Hasanen, N. Honkanen, P. Poffenberger, M. Roney (Victoria); S. Bhadra, S. Galymov (York); P. Birney, A. Dowling, R. Langstaff, M. Lenkowski (TRIUMF/Victoria).

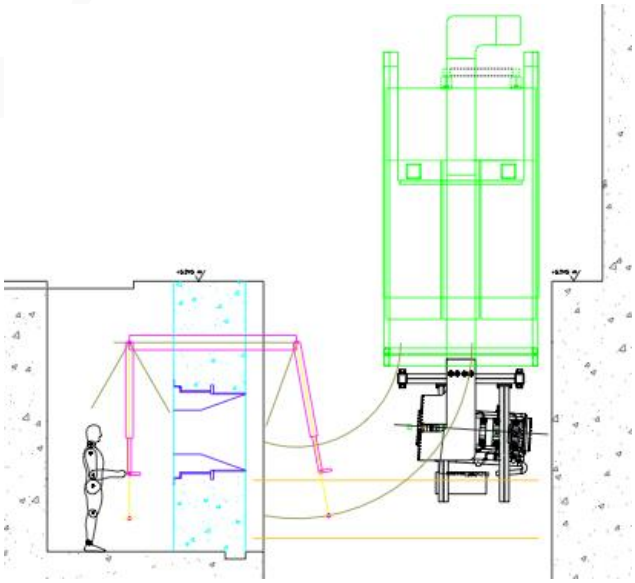

Fig. 1. Remote handling manipulator design for the T2K target station.

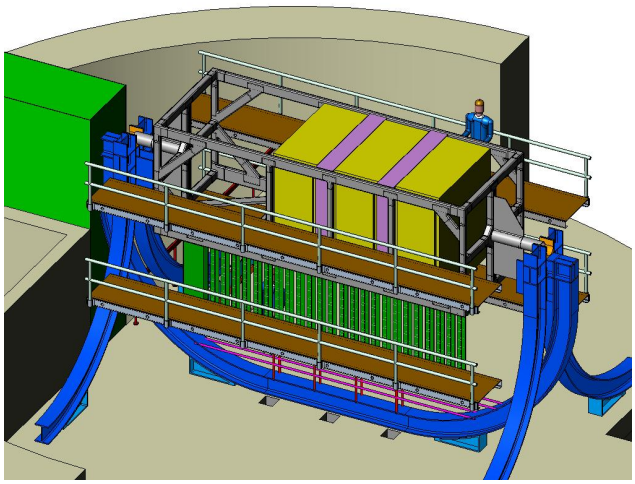

Fig. 2. TPC and FGD supported inside the ND280 magnet.

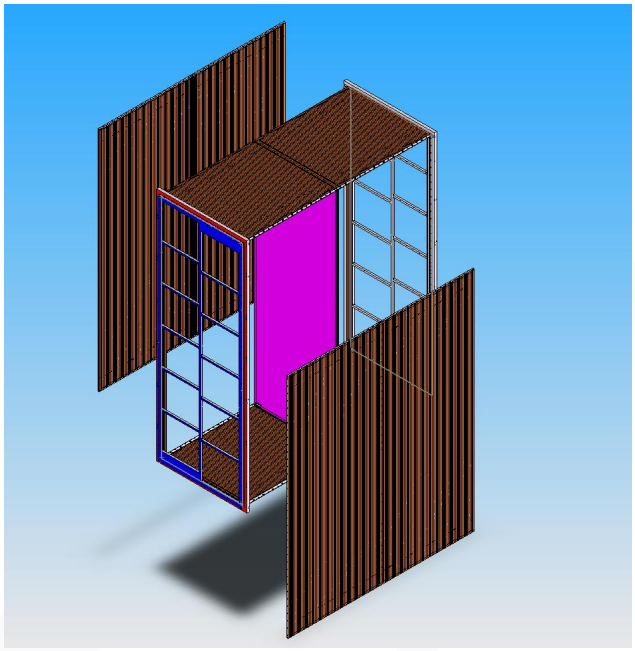

Fig. 3. 3D drawing of the TPC field cage.

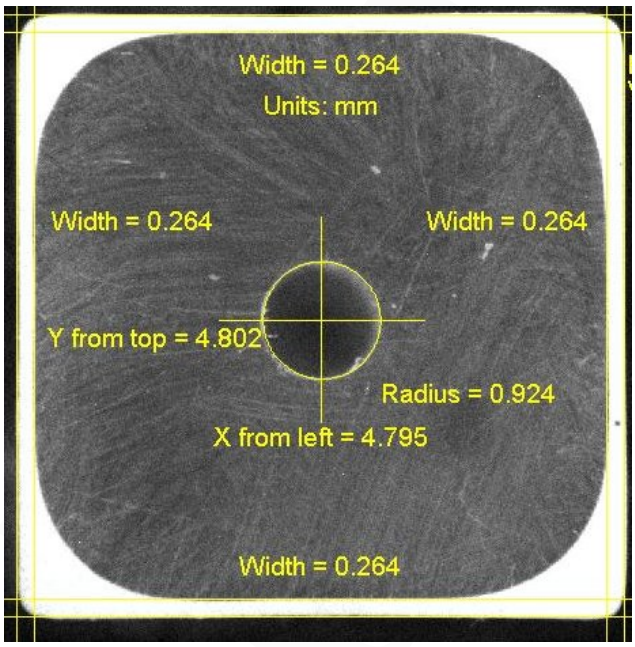

Fig. 4. Cross section view of the extruded scintillator.

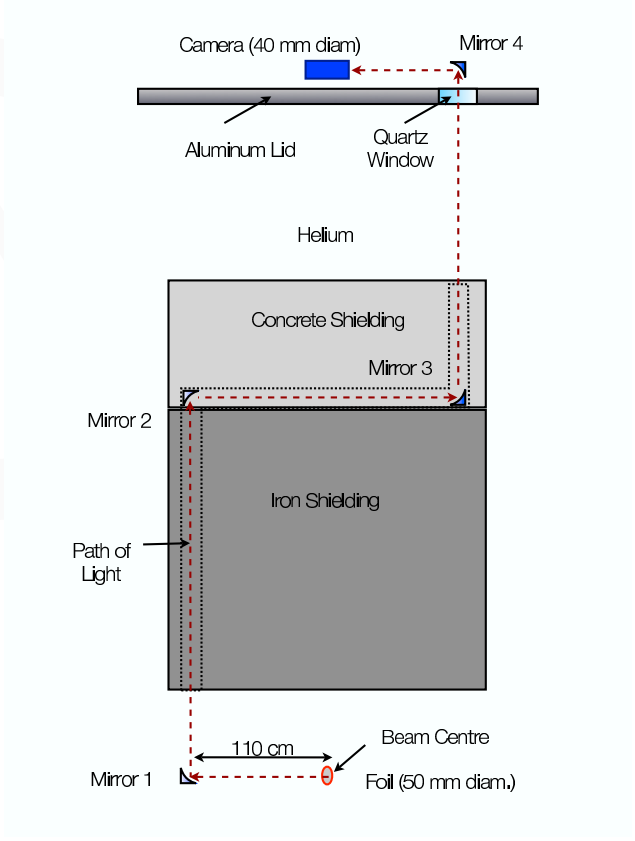

Fig. 5. The optical path of the OTR system. The beam travels through the foil, into the page.